공학박사 학위논문

Construction of Surface Nanostructures and Nanonetworks based on Assembly of Colloidal Particles

콜로이드 입자 자기조립 기반의 표면 나노구조물 및 나노네트워크 형성 기술 연구

2013 년 8 월

서울대학교 대학원

공과대학 전기컴퓨터공학부

박 승 철

Construction of Surface Nanostructures and Nanonetworks based on Assembly of Colloidal Particles

지도교수 이 신 두

이 논문을 공학박사 학위논문으로 제출함

2013 년 8 월

서울대학교 대학원

공과대학 전기컴퓨터공학부

박 승 철

박승철의 박사 학위논문을 인준함

2013 년 6 월

위 원 장 박 남 규 (인)

부위원장 이 신 두 (인)

위 원 김 성 재 (인)

위 원 최 종 선 (인)

위 원 배 진 혁 (인)

Abstract

Construction of Surface Nanostructures and Nanonetworks based on Assembly of Colloidal Particles

Seung Chul Park

School of Electrical Engineering and Computer Science

The Graduate School

Seoul National University

Recently, surface nanostructures and nanonetworks have extremely much attention for core element in diverse fields such as optics, electronics, plasmonic, and photonics. Since the surface nanostructures can generate the non-linear optics, for example, meta-materials for optical cloaking and collective oscillation of electrons for plasmonic detection, and band-gap tuning such as extraordinary transmission of light, the construction of surface nanostructures might be the key factor for various applications. In addition, surface metal nanonetworks can be applied not only the electrode in electronic devices but also the functional element in opto-electronic devices which are the organic light emitting diode and organic photo-voltaic. Therefore, for application of various fields, construction of surface nanostructures and

nanonetworks with various sizes, shape, and periodicity for special functionality should be established.

In this thesis, new platform for construction of surface nanostructures and nanonetworks with metal or nonmetal materials based on self-assembled colloidal particle are presented for the various sizes, shapes, and periodicities of surface metal or nonmetal nanostructures and nanonetworks. First, the general overview of the construction methods for surface nanostructures and nanonetworks and the construction methods based on the colloidal particle assembly as bottom-up approach are introduced. Especially, the convective method for self-assembled colloidal particle platform is presented. In addition, it is presented that the underlying physical mechanism comes from the interface between the colloidal particles on substrate.

In the viewpoint of the surface nanostructure formation, combination of the self-assembled colloidal particles and functional fluids for the formation of surface nanostructures and nanonetworks is demonstrated. The interaction between the functional fluids and self-assembled colloidal particle is known as liquid bridging phenomenon. The liquid bridging phenomenon can help to make surface nanonetwork of functional fluid by spontaneous distribution between the colloidal particles. The surface nanonetworks by functional fluids can be applied not only as the nanomesh structure by Ag ink but also sacrificial layer for surface nanodots formation. By the basic principle of liquid bridging phenomenon, the relationship between the size of colloidal particle and the thickness of functional fluid should be considered for surface

nanodots and nanomesh formation. In addition, size scalable conducting nanonetwork electrode can be formed by using the functional fluid formation on Au electrode. The formation of functional fluid on Au electrode can be the sacrificial layer against the etching process that the selective etching process can induce the Au electrode. The selective etching process on Au electrode can make the various sizes of pores with nano-range periodicity by control the etching time. This size scalable conducting nanonetwork electrode might be the key element in opto-electronic devices.

Next, combination of the self-assembled colloidal particles and metal layer for the formation of surface nanostructures and nanonetworks is demonstrated. Using the self-assembled colloidal particles as the sacrificial layer in lift-off process after metal deposition, the surface metal nanostructures can be generated. The self-assembled colloidal particles on substrate are arranged as a close-packed monolayer formation which has the void space between the neighboring colloidal particles. When the metal layer is deposited on the substrate, the metal nanostructures which are positioned between the colloidal particles are remained on substrate after the detachment of colloidal particle. This method which is known as nanosphere lithography can provide triangular shaped surface metal nanostructure with various size and periodicity by altering the size of colloidal particle. Such the surface metal nanostructures are employed key element of various applications including plasmonics and photonics. In addition, self-assembled colloidal particle can be the platform of not physically formation of functional fluid but also the optically modulation of light pathway when the metal layer are

deposited on the self-assembled colloidal particles. Due to the spherical shape of colloidal particles, the pathway of light which pass through the colloidal particle can be modulated. The modulation of light pathway can focus the light in small area that such focusing of light can generate the small feature size of photoresistor. It is also can control the amount of focusing ratio by altering the thickness of metal layer which can block the penetration of light. Using this focusing effect of colloidal particles, patterned photoresistor on substrate can be achieved that the reversal patterns which are surface structure and patterned electrode can be formed by lift-off process and etching process, respectively.

Moreover, it is presented that the surface nanostructure is formed by the colloidal particle itself. Using the structural deformation by the thermal treatment, the colloidal particles arranged on substrate can be applied as the surface nanostructure for nanotopography. Such the surface nanotopography can be the platform interaction between the surface nanostructure and nanomaterials such as liquid crystals (LCs) or biomaterials. The interaction between the surface nanostructures and LCs can change the distribution of nanomaterials on substrate that the variation of optical characteristic of device can be achieved.

In conclusion, though this thesis, it is presented that the various construction methods of surface nanostructures and nanonetworks based on the self-assembled colloidal particles and its applications. Various construction methods of various size, shape, and periodicity of surface nanostructures and nanonetoworks, introduced here, are expected to provide a

basis for realizing many applications in various fields. Moreover, the basic principle and construction technique for construction of surface nanostructures and nanonetworks will provide a platform for the opto-electronic devices.

Keywords: colloidal particles, surface nanostructures, surface nanonetworks, interfacial interactions, opto-electronic device, biosensor application

Student Number: 2007-20978

Contents

List of Tables

List of Figures

Chapter 1. Introduction

1.1 Importance of Surface Nanostructures and Nanonetworks

Recently, the advances in nanotechnology have led to open new research fields on nanometer scales, for example, the collective oscillation of electrons in nano-sized noble metals [1-3], the negative refractive indices in stacked nanostructures composed of metals and dielectric materials [4-6], the super-hydrophobicity on nanostructured surfaces [7, 8], and fluidics having extremely large surface-to-volume ratios [9, 10]. One of the central issues in such new areas concerns how to construct functional nanostructures and nanonetworks of metals, dielectrics, or composite materials. Since the unique properties mentioned above depend on the structural properties which are the size, shape, and periodicity of surface nanostructures and nanonetworks, construction method with various structural conditions should be established [1-3, 11-13]. In addition, the surface nanostructures and nanonetworks on substrate should be made by various materials not only the metals but also the dielectric materials. Since the materials have own characteristics such as conductivity, rigidity, and solubility, the construction method should be suitable for various materials formation. Therefore, new platform of

constructing surface nanostructures and nanonetworks with various structural conditions and materials is strongly required.

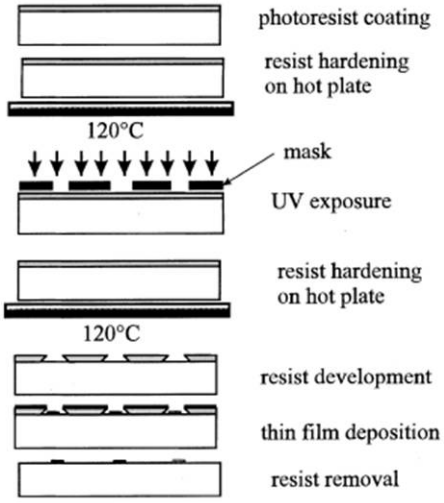

Figure 1. 1 Construction method based on photolithography.

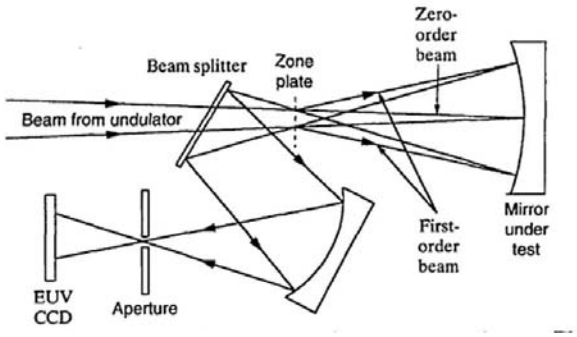

Figure 1. 2 Construction method based on E-UV.

1.2 Construction Methods of Surface Nanostructures

1.2.1 Conventional methods

The conventional methods are consisted of the top-down approaches and bottom-up approaches. The top-down approach often uses the traditional fabrication methods where externally controlled tools are used to cut, mill, and shape materials into the desired shape and order. These methods have common procedure for fabricating surface structures. First, the target material for surface structures is formed on the whole substrate. Using various methods including etching, lift-off, milling, and polishing method, the size of material with whole area is reduced.

There are several methods of top-down approach including photolithography [14, 15], electron beam lithography [16, 17], extreme ultraviolet (E-UV) lithography [18], and focused ion beam (FIB) milling method [19]. The photolithography is well established method for constructing microstructure. The photoresistor which is the material of photosensitization is applied as the sacrificial layer of lift-off process or pre-patterned buffer layer of shadow mask effect. Figure 1.1 shows the formation of surface structure using the photolithography. This method can construct surface structure on large area easily but the feature size is limited in a few micrometer ranges. To overcome such limitation of feature size, the shorter wavelength of exposed light should be employed, since the feature resolution depends on the half of the wavelength. The E-UV lithography (Fig. 1.2) and electron beam

lithography (Fig.1.3) are the lithographic method with the short wavelength of UV and electron. Due to the short wavelength, the feature size is decreased from tens to hundreds of nanometer range. Though this method can generate the surface nanostructures on substrate, the high-cost and low throughput problems are still remained. In addition, FIB milling method is the directly writing method by elimination of un-patterned material for desired shape as shown in Fig.1.4. This method also has the small feature size with a few nanometers to micrometers. However, similar to other method, this FIB milling method also has the same weakness in cost-effective and throughput.

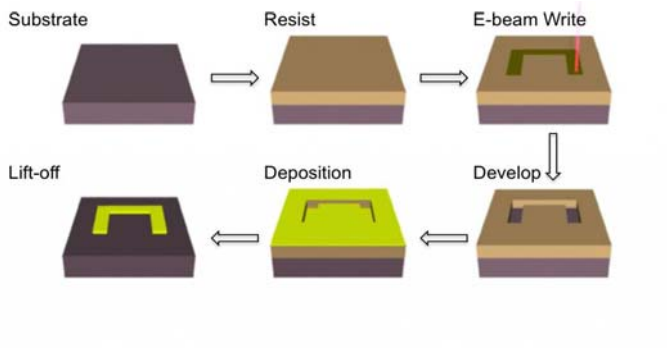

Figure 1. 3 Construction method based on E-beam lithography.

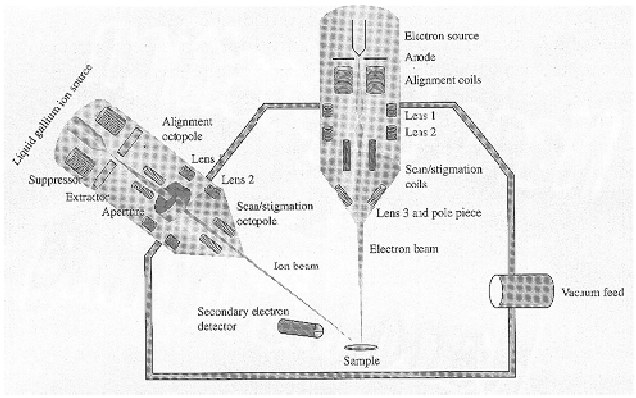

Figure. **A FIB instrument showing the ion and Electron columns and the specimen inside the vacuum chamber**

Figure 1. 4 Construction method based on FIB milling.

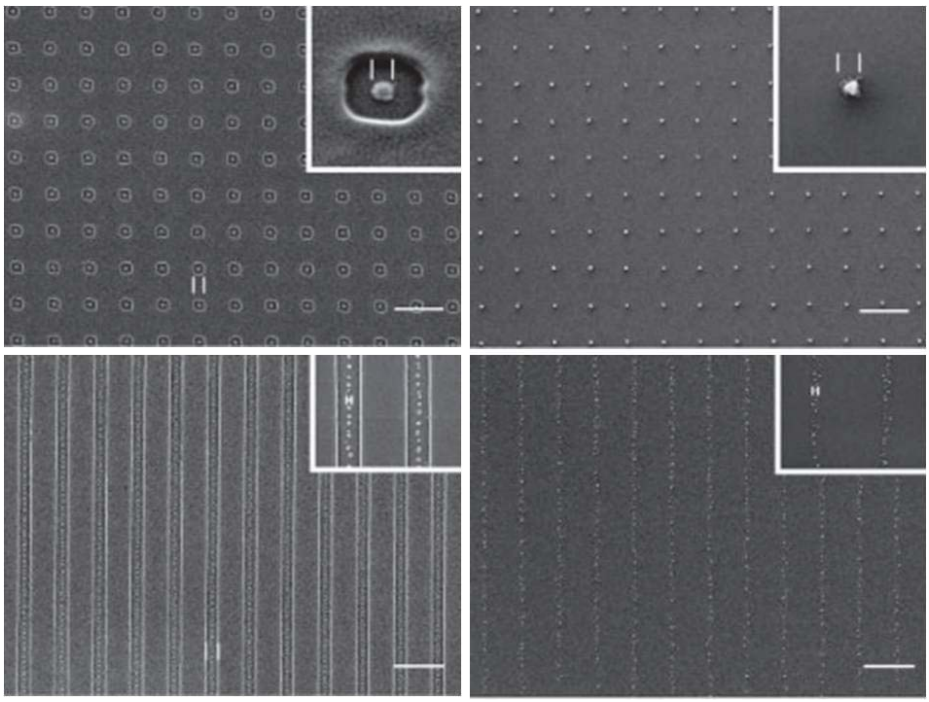

Figure 1. 5 Construction method based on colloidal particle distribution.

The bottom-up approaches, in contrast to top-down approaches, use the elements of building blocks for surface nanostructures and nanonetworks by self-assembly [20-22], soft lithography [23-25] including stamping method [26, 27], direct writing [28], or molecular recognition [29]. These bottom-up approaches are mainly discussed by replacing the conventional top-down approaches since the surface nanostructures are constructed easily on large area by the assembly of the basic elements with nano-sized. There are several methods using the basic principles mentioned above are studied. First, the self-assembly of nanomaterials which are the colloidal particle of metal or nonmetal can be used for construction of surface metal or nonmetal nanostructures as shown in Fig. 1.5 [30]. Though this method can make surface nanostructures and nanonetworks on large area with nanomaterials easily [31], the structural properties which are the size and shape are fixed by the original structural properties of core elements. In addition, the position of the self-assembled materials on substrate cannot be easily controllable that the additional processes which are the pre-patterned substrate and confine the evaporating direction by microstructures are needed [32-35].

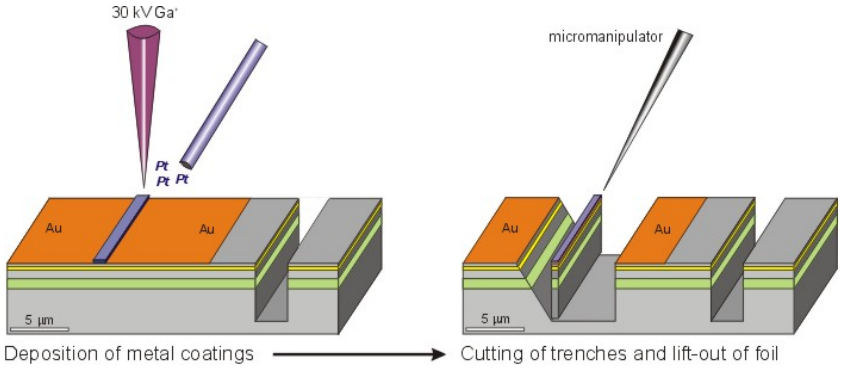

Figure 1. 6 Construction method based on FIB.

Another case, in Fig. 1.6, FIB with direct writing of metal material also can be used for construction of surface nanostructure and nanonetworks. This method can provide the various sizes, shapes, and positions of surface structure form nanometer to micrometer range. However, this method also is limited in low throughput and small area. The other case is the molecular recognition such as block co-polymer and phase-separation based construction method as depicted in Fig.1.7. This method also can make various sizes of nanostructures on substrate. However, there is a material limitation in block co-polymers and phase-separation materials. Therefore, for construction of surface nanostructures and nanonetworks, new platform with various materials, structural properties, easy process, and cost-effective should be set up.

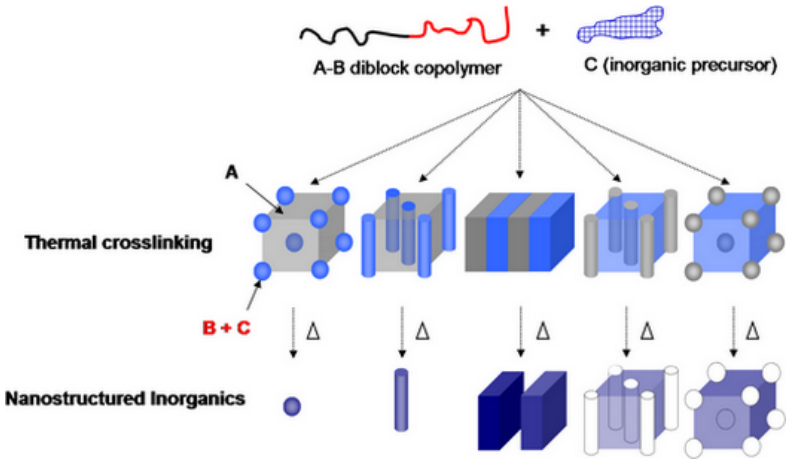

Figure 1. 7 Construction method based on molecular recognition.

1.2.2 Colloidal particle based construction methods

The self-assembly of colloidal particles can be applied for the surface nanostructure and nanonetwork by itself. Using the pre-patterned substrate to control the distribution of colloidal particles, the surface nanostructure on substrate can be achieved as shown in Fig. 1.8. In addition, using the limitation of the evaporation direction by microstructure, nanonetwork of colloidal particles can be formed since the colloidal particles are dispersed in solvent [36]. (Fig. 1.9) These construction methods using colloidal particle as the basic element of structure can make various size and shape of surface nanostructure. However, these methods which construct the surface nanostructure and nanonetworks of colloidal particles have the weakness in long-term stability by the physisorbed nanoparticles. Moreover, the pre-patterned substrate for the positioning the colloidal particles as the surface nanostructure is also required the additional process to fabricate.

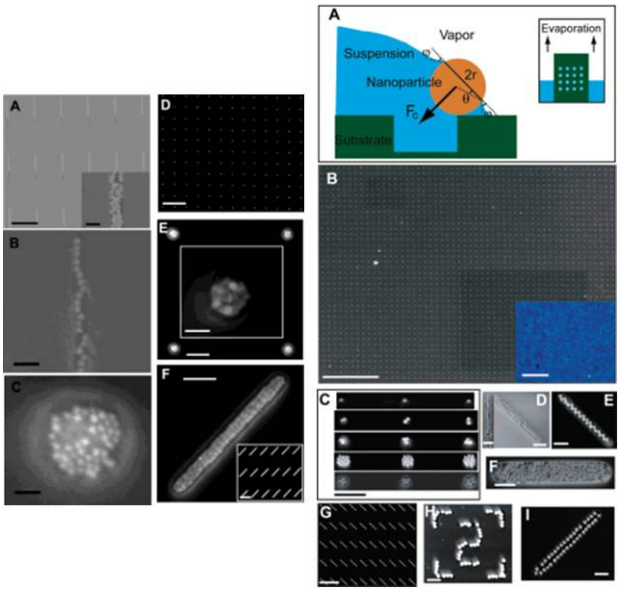

Figure 1. 8 Construction method based on template with colloidal particle.

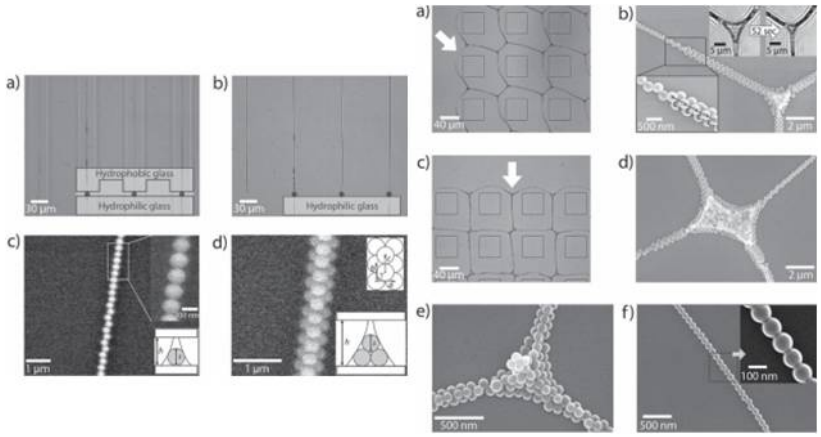

Figure 1. 9 Construction method based on evaporating.

For the conquest of the weaknesses, there is a new method of surface nanostructure and nanonetwork formation using colloidal particle as the template of another material formation. The close-packed colloidal particles are arranged by convective method [37]. Since the colloidal particles are dispersed in solvent, the evaporation of solvent with inclined meniscus, the dispersed colloidal particles are dragged into the edge of meniscus. Therefore, when the various conditions such as the evaporating rate, inclined meniscus, and size of colloidal particle are balanced, the close-packed monolayer formation can be achieved, as shown in Fig. 1. 10.

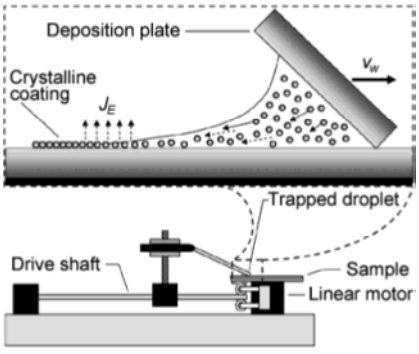

Figure 1. 10 Convective method.

First, using the close-packed colloidal particles on substrate, the metal layer is deposited on substrate. The metal nanostructures are formed on the void space between the neighboring particles. After the detachment of colloidal particle, the metal nanostructures are still remained on substrate. This method is the nanosphere lithography as shown in Fig. 1.11 [38]. The colloidal particle can be applied as the buffer layer against the metal deposition. Using this method with etched colloidal particle, the deposited metal layer is connected each other that the metal nanonetwork formation can be produced as shown in Fig. 1.12 [39]. This metal nanonetwork formation can be the key element in opto-electronic devices. In addition, the template of close-packed colloidal particle can limit the evaporation of solvent that the nanomaterials dispersed in solvent can be patterned on substrate as shown in Fig. 1.13 [40]. These methods using the template of colloidal particle for construction surface nanostructures and nanonetworks of other materials might be the practical and critical method of surface nanostructures and nanonetworks formation.

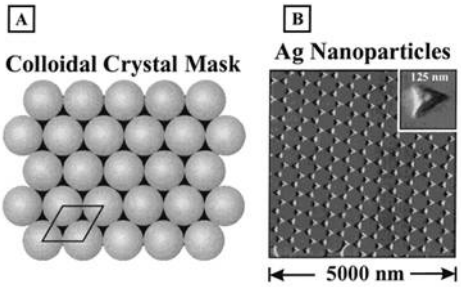

Figure 1. 11 Nanosphere lithography.

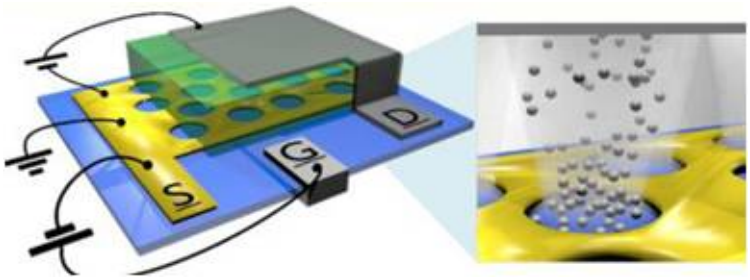

Figure 1. 12 Construction method using etched colloidal particle.

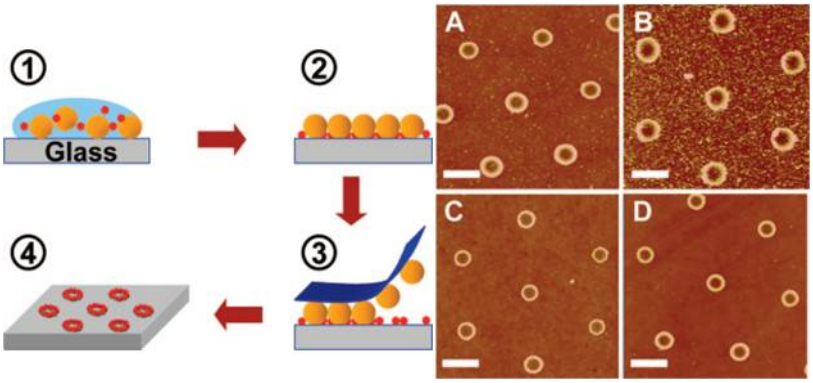

Figure 1. 13 Colloid template for nanomaterial formation.

1.3 Outline of Thesis

This thesis contains five chapters including **Introduction** and **Conclusion**. As an introductory part, **Chap. 1** provides the brief introduction of surface nanostructures and nanonetworks and the various construction methods. The general principles and key factors of surface nanostructures and nanonetworks

formation are introduced. The motivation of this research on the construction method based on the self-assembled colloidal particles is also introduced.

In **Chapter 2**, the construction of surface nanostructures and nanonetworks based on the liquid bridging phenomenon of functional fluids on self-assembled colloidal particles is introduced. The self-assembled colloidal particles can be applied to pattern the functional fluids by regulating the spontaneous formation. Using the Ag ink which the Ag nanoparticles are dispersed in solvent as the functional fluid, the surface nanonetwork of metal mesh can be achieved. In addition, size scalable conducting nanonetwork electrode can be constructed by selective etching process with liquid bridging of the fluorinated polymer on substrate. By applying the etching process, the contact area between the colloidal particle and substrate is etched while the other region is remained. This method can construct various sizes of conducting nanonetworks by control the time of etching process and altering the size of colloidal particles. Moreover, using the photoresistor and fluorinated polymer as the functional fluids to form the sacrificial layer of lift-off process, surface nanostructures of metal dots can be produces after the thermally deposition and removal of sacrificial layers. This method based on the liquid bridging in self-assembled colloidal particles can construct various sizes of nanomesh and nanodots.

In **chapter 3**, the deposited metal on the self-assembled colloidal particle is introduced. Using the surface metal nanostructure, the plasmonic biosensing application can be produced. Since the metal nanostructure of Au can generate the localized surface plasmon resonance in visible light range,

the nanostructures made by detachment of colloidal particle can be applied to plasmonic biosensor. For the plasmonic detection in biomimic environment, the supported lipid bilayers are formed on the substrate with surface metal nanostructure. The formation of supported lipid bilayers and the protein binding event can affect the plasmonic behavior that the plasmonic detection can be achieved. Second, when the metal deposited on the self-assembled colloidal particles, the substrate can be applied as the optical lithographic mask. In addition, by detachment of colloidal particles after the metal deposition, the metal nanostructures are formed on substrate. For the practical applications, first, using the deposited metal on the self-assembled colloidal particle, the light can pass through the self-assembled colloidal particle with focusing effect due to the spherical shape of colloidal particle. Using such focusing effect, the size of photosensitization in photoresitor can be controlled. This method can construct various size of surface structure by regulating the metal thickness which can block the light.

In **Chapter 4**, the surface nanotopography by thermal fixation of colloidal particle is introduced. First, it is presented that the formation of surface nanostructure using polystyrene particle. For strong fixation and size scalability of colloidal particle structures, the thermal treatment induced with various times. Using the constant volume model and spherical approximation, the structural dimension dependency of the induced time can be proved. Next, for figuring out of the interaction between the surface nanostructures of thermally treated colloidal particles and liquid crystals, the substrates with nanostructure are assembled and the liquid crystals are filled in the cell. The

iso-contrast characteristics can show the local distribution of liquid crystals on nanostructures that the symmetry viewing angle liquid crystal display can be achieved.

Finally, **chap. 5** gives brief summary and some concluding remarks for this thesis.

Chapter 2. Nanonetwork by Liquid Bridging

2.1 Introduction

Recently, the advances in nanotechnology have led to open new research fields on nanometer scales, for example, the collective oscillation of electrons in nano-sized noble metals [1-3], the negative refractive indices in stacked nano-structures composed of metals and dielectric materials [4], the super-hydrophobicity on nano-structured surfaces [8], and fluidics having extremely large surface-to-volume ratios [10]. One of the central issues in such new areas concerns how to construct functional micro to nanostructures of metals, dielectrics, or composite materials. In fabricating those functional structures, solution-based processes are, in principle, very simple and cost-effective but have not been fully explored so far. The most promising approach relies on an ink-jet printing method which has been widely employed for organic electronics of low cost and flexibility [41-43] but limits the feature resolution to several micrometers [44-46]. Thus, it is important to search for a new methodology of building up nanostructures from different classes of functional solutions.

In this chapter, a simple generic principle of constructing periodic nanomesh structures and nanodots arrays on the basis of liquid bridging in particle self-assemblies is demonstrated. In our study, the self-assemblies of nano- to micro-sized spheres of polystyrene, produced in a close-packed monolayer on

a substrate by a convective method, are used as templates for liquid bridging of a variety of functional fluids in the pores among the neighboring particles. As one class of nanostructures, a mesh structure is directly obtained after the solidification of the fluid, followed by the detachment of the particles from the substrate. As another class, a periodic dot array is produced when a mesh structure of a sacrificial material is removed through a lift-off process after deposition of a desired substance. The generic principle is demonstrated in various types of nano-mesh structures of silver-ink and nano-dot arrays of gold. The physical features of the nano-structures are found to depend on the size of the particle, the crystal structure of the particle assembly, and the volume occupied by liquid bridging.

2.2 Liquid Bridging

A basic concept of liquid bridging between two colloidal particles in contact was previously reported [47, 48], as shown in Fig 2.1. The liquid bridging phenomenon is the fluid connection by the interaction between the fluid and solid structure. The previous reports are based on the fluid connection between the solid structures which are the neighboring two particles or upper and lower flat substrates. The liquid between the solid are connected by the properties such as viscosity and surface tension. By the expansion of this principle, the self-assembled colloidal particle on bottom substrate can be applied as the upper solid structure that the liquid bridging phenomenon between the flat bottom substrate and the assembled colloidal particle can be generated. Since the liquid bridging can be occurred between two solids, the

template of liquid bridging between the substrate and colloidal particle can also be provided. In addition, the self-assembled colloidal particles have the periodic cavities between the neighboring particles spontaneously that the cavities can generate the capillary force which can keep the fluids in them. Using such template of self assembled colloidal particle, various functional fluids can be formed spontaneously.

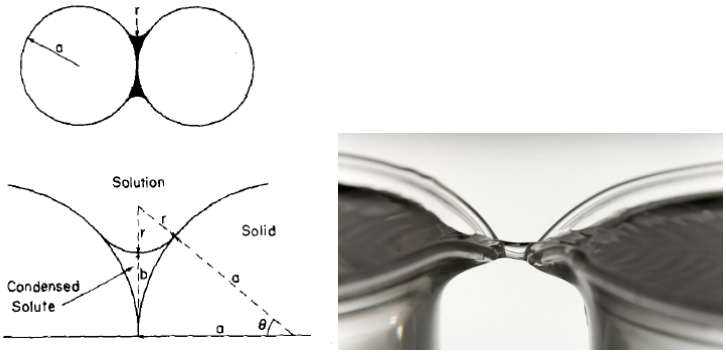

Figure 2. 1 Liquid bridging between two solids.

For the formation of self-assembled colloidal particle as the template of liquid bridging, the convective method is employed as shown in Fig. 2.2. The colloidal solutions of the PS spheres of four different sizes (d = 500 nm, 1 μm, 10 μm, and 25 μm) were used for producing self-assemblies in a closed-packed monolayer. The PS spheres were initially dispersed in water with a detergent (surfactant) which stabilizes the colloidal dispersion. Before using each colloidal solution, water containing the detergent should be replaced by distilled water. The colloidal solution of about 1 wt % was centrifuged at 10000 rpm for 10 min for the sedimentation of the PS particles, water

containing the detergent was replaced by DI water in about 3 wt % at which the uniform monolayer was formed in our case, and the ultra-sonication process was finally carried out for 10 min for colloidal dispersion. The colloidal particles in DI water were then dip-coated on a hydrophilic glass substrate. The substrate with the self-assembled PS particles in monolayer was baked at 65°C for 120 min to remove residual DI water and a functional fluid was spin-coated directly on it.

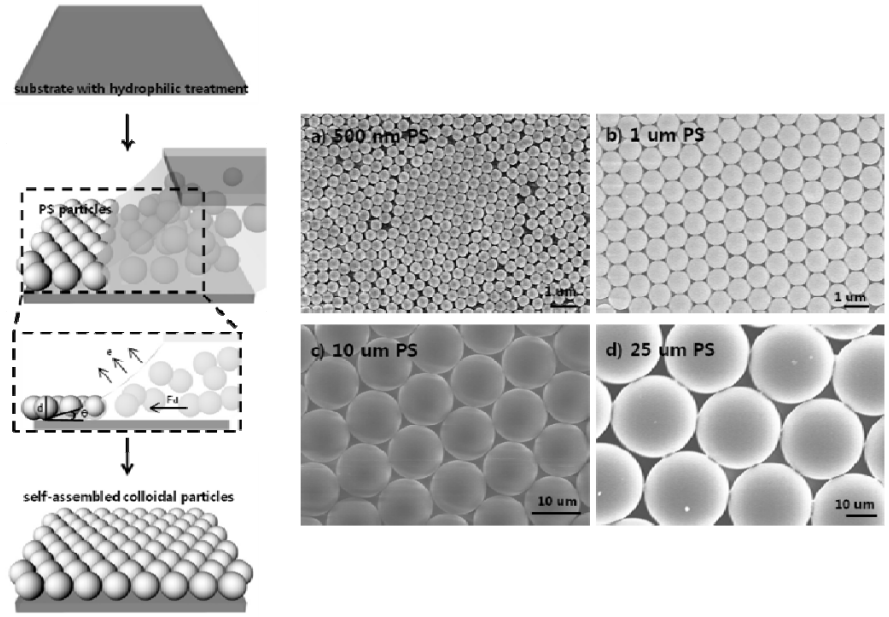

Figure 2. 2 Schematic diagrams of convective method and the scanning electron microscope images of self-assembled colloidal particle with various sizes.

2.3 Liquid Bridging of Various Functional Fluids

Figure 2.2 shows the underlying concept of constructing periodic nanostructures by liquid bridging in a particle self-assembly used as a

template. As shown in Fig. 22, the self-assembly of nano- to micro-sized spheres of PS is first produced in a close-packed monolayer on a hydrophilic substrate by a convective method from a colloidal solution of the PS particles dispersed in water. Note that the size of the PS particle, the coating speed (v), and the evaporation rate influence the layer structure as well as the packing density during self-assembling. Both the shape of the water meniscus and the evaporation rate play a critical role in the formation of a close-packed monolayer structure. For smaller particles, a faster coating speed is desirable to form the monolayer structure.

A functional fluid is subsequently coated onto the template of self-assembled particles in Fig. 2.2. Depending on the diameter (d) of the PS sphere and the volume occupied by the liquid (in terms of the height h) in the pores among the neighboring particles in the monolayer, different types of liquid bridging will occur. Three examples of $h/d << 1/2$, $h/d \sim 1/2$, $h/d > 1$ are schematically shown in Fig. 2.3. The partial coverage by liquid bridging ($h/d < 1/2$) is desirable to generate solidified fluid patterns after the detachment of the particles. As shown in the last schematic diagram in Fig. 2.3, periodic functional patterns in a mesh-structure are finally produced. It should be noted that the case of $h/d > 1$ corresponds to the complete coverage of the fluid over the particle self-assembly. The pore size surrounded by the nearest-neighbor particles, the viscosity of the fluid, and the strength of the capillary force will primarily determine the coverage of the fluid by liquid bridging in the template.

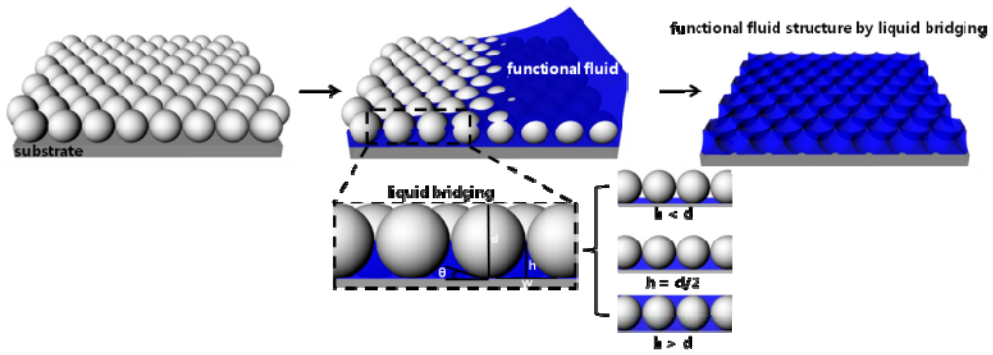

Figure 2. 3 the underlying concept of liquid bridging of a functional fluid in a self-assembled particle template for the construction of a mesh structure.

2.3.1 Metal dispersion solution

The Ag ink which the Ag nanoparticles are dispersed in solvent is used as the functional fluid of liquid bridging. The Ag ink is spin coated on the self-assembled colloidal particle with various *Rs* such as 1000, 3000, and 7000 rpm. The natural thickness of Ag ink on the substrate was measured to be about 1 μm at *Rs* = 3000 rpm. Thus, as shown in the SEM images in Figs. 2.4(b) and (c), at *Rs* = 3000 rpm, the full coverage of Ag ink was necessarily produced in two cases of *d* = 500 nm and 1 μm below the natural thickness. However, for the cases of *d* =10 and 25 μm, the partial coverage of Ag ink was achieved by liquid bridging and the mesh structure with hemispherical pores was very well developed as shown in the SEM images in Figs. 2.4(d) and (e). The mesh structure of Ag ink was accordingly obtained after the subsequent removal of the PS particles with the treatment of the substrate in toluene. Since the height and line width of the mesh depends on *Rs*, the *Rs* is changed in the range from 1000 rpm to 7000 rpm.

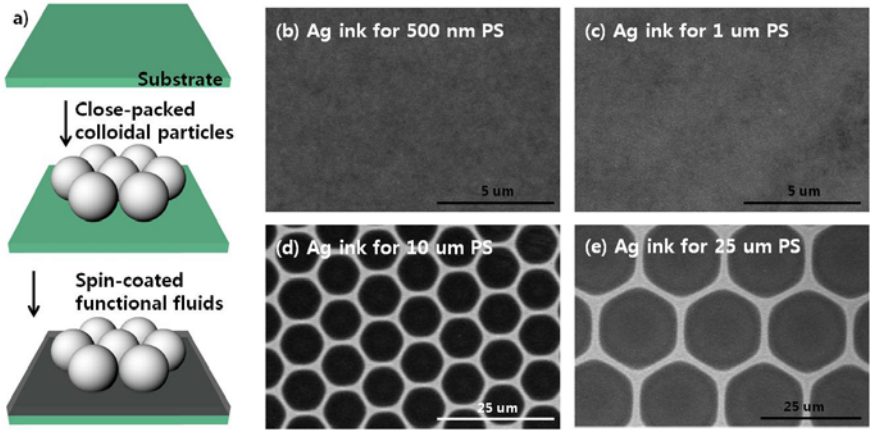

Figure 2. 4 (a) The schematic diagram of Ag ink pattern and SEM images of Ag ink patterns by liquid bridging in the templates of the self-assembled PS particles of (b) 500 nm, (c) 1 μm, (d) 10 μm, and (e) 25 μm in diameter. The insets illustrate schematically the side views of the PS particles that are liquid-bridged in terms of the relative height of Ag ink

2.3.2 Polymer solution

The liquid bridging phenomena of two different sacrificial materials, AZ-1512 and EGC-1700, is applied with depending on the relative height of the fluid occupied in the pores and the diameter of the PS particles ranging from 500 nm, 1 μm, 10 μm, and 25 μm. For AZ-1512, it is clear from the SEM images in Figs. 2.5(a)-(d) for different values of d that the partial coverage ($h/d < 1/2$) of the fluid by liquid bridging in the PS template was barely obtained below d = 10 μm at Rs = 3000 rpm due to the high viscosity. However, for EGC-1700, being used as a sacrificial material [49-51], it was easily achievable down to d = 1 μm at the dip-coating speed of 100 mm/min due to low viscosity as shown in the SEM images in Figs. 2.6(a)-(d) for

different values of d. The insets in Figs. 2.5 and 2.6 illustrate schematically the side views of the PS particles that are liquid-bridged in terms of the relative height of the fluid. Note that under the coating conditions used for each sacrificial material, the natural thickness of AZ-1512 on the glass substrate was about 1.2 μm and that of EGC-1700 was about 100 nm. This suggests that for the partial coverage of the fluid in the template of a closed-packed monolayer, the size of the particle should be at least several times larger than the natural thickness of the fluid on the substrate. In addition, for lower viscosity and higher coating rate, higher resolution of the solidified fluid nanostructure will be available by liquid bridging.

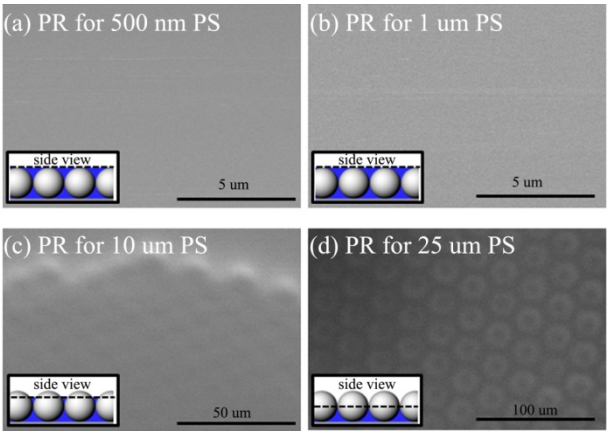

Figure 2. 5 The SEM images of AZ-1512 photoresist patterns by liquid bridging in the templates of the self-assembled PS particles of (a) 500 nm, (b) 1 μm, (c) 10 μm, and (d) 25 μm in diameter. The insets illustrate schematically the side views of the PS particles that are liquid-bridged in terms of the relative height of AZ-1512.

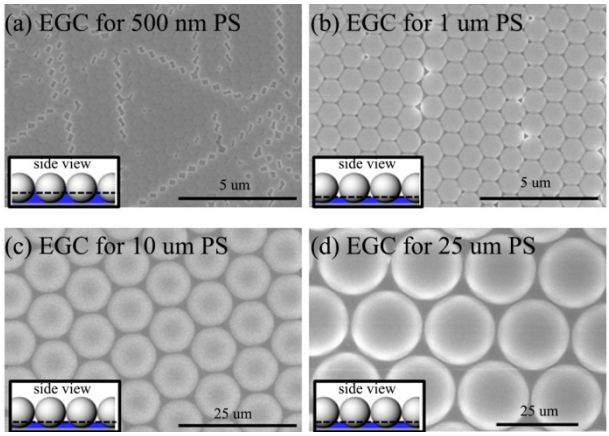

Figure 2. 6 The SEM images of EGC-1700 polymer patterns by liquid bridging in the templates of the self-assembled PS particles of (a) 500 nm, (b) 1 μm, (c) 10 μm, and (d) 25 μm in diameter. The insets illustrate schematically the side views of the PS particles that are liquid-bridged in terms of the relative height of EGC-1700.

Based on the above results, mesh-structures of AZ-1512 photoresist and EGC-1700 were produced using the PS particles with d = 10 and 25 μm for EGC-1700 and those with d = 500 nm and 1 μm for EGC-1700. In both cases, the substrate was treated with toluene for 5 min to remove the PS particles from the solidified fluid mesh-structures. As clearly seen from the SEM images in Figs. 2.7(a) and (b), two different micro-meshes with hemispherical pores of AZ-1512 were well formed. The nano-meshes of EGC-1700 were shown in the SEM images in Figs. 2.7(c) and (d). The insets in Fig. 2.7 represent the side views of the AZ-1512 and EGC-1700 mesh patterns with hemispherical pores produced by liquid bridging. It should be noted that the feature size (or the pattern resolution) in the mesh-structure is predominantly governed by the natural thickness of the fluid on the substrate, depending on the interfacial

properties, the intrinsic viscosity, the coating speed, and the evaporation rate, as discussed above.

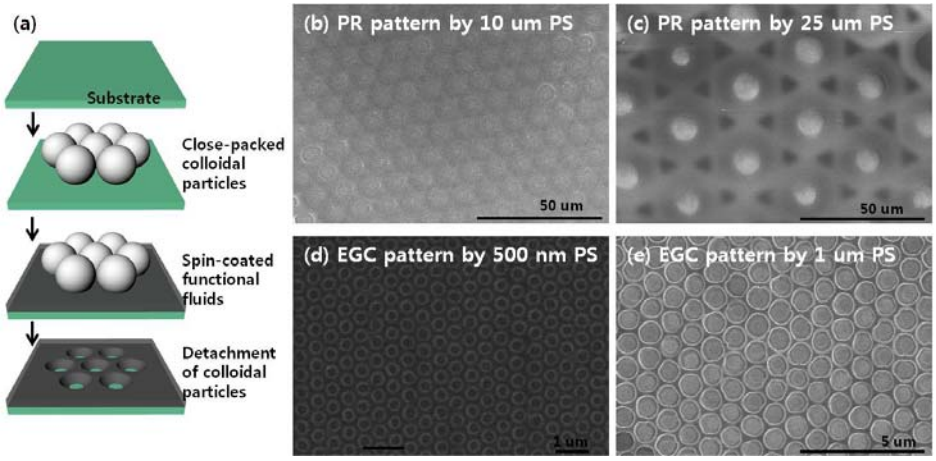

Figure 2. 7 The schematic diagram of functional fluid pattern and SEM images of the solidified AZ-1512 patterns after the removal of the PS particles of (a) 10 μm, and (b) 25 μm in diameter. The SEM images of the solidified EGC-1700 patterns after the removal of the PS particles of (c) 500 nm and (d) 1 μm in diameter. The insets represent the side views of the AZ-1512 and EGC-1700 mesh patterns with hemispherical pores produced by liquid bridging.

2.4 Nanonetwork Formation

Recently, conducting nanonetworks have extremely attracted much attention for not only the replacement of transparent electrode which is currently made by indium-tin-oxide (ITO) but also the core element of various fields due to the unique characteristics of conducting networks

in nano-scale. For the replacement of the ITO, there are several approaches such as carbon nano-tube (CNT) based construction method. The CNT is the ideal material for conducting layer due to the high electric conductivity ($10^{-4}\Omega$Cm) and the high ratio of surface area to volume. However, the CNT material should be dispersed in solvent to for transparent electrode. After the dispersion process, the solution should be coated on glass substrate. Though the dispersion and coating process can generate the transparent electrode, the problem of random distribution of CNT and lack of uniformity still remained. To overcome such weaknesses, various coating and formation method including laser assisted CNT deposition and chemical vapor deposition of CNT are studied recently. In addition, for realization of transparent electrode, the graphene based construction method is established. Though the graphene also can be applied for the transparent electrode due to the high electron mobility (150 times faster than silicon) and high transmittance (98%), this material has the same weaknesses of CNT since the graphene should be dispersed in solvent for application. Another approach is the conducting polymer based construction method. The simple coating process of PEDOT:PSS can provide the transparent electrode on substrate. However, the material of conducting polymer can induce the damage to other organic material due to the chemical property (pH 1.5~2). Therefore, new approach for

construction of transparent electrode with simple and easy process should be established.

2.4.1 Period nanomesh of Ag ink

The SEM images of the Ag mesh structures produced using the PS particles of d = 10 and 25 μm at three different values of Rs = 1000, 3000, and 7000 rpm were shown in Figs. 2.8(b) and 8(c), respectively. The corresponding geometrical profiles (scanned along the white dashed lines) of a single Ag mesh line having a trapezoidal cross-section were also shown. For d = 10 μm, the height of the Ag mesh was h = 2.7, 1.6, and 640 nm at Rs = 1000, 3000, and 7000 rpm, respectively, as shown in Fig. 2.8(b). The line width was w = 2.4, 2.3, and 720 nm for Rs = 1000, 3000, and 7000 rpm, respectively. At higher Rs, lower h and narrower w were obtained. For d = 25, as shown in Fig. 2.8(c), h = 6.4, 3.0, and 1.2 μm at Rs = 1000, 3000, and 7000 rpm, respectively. The line width was w = 8.9, 2.5, and 780 nm at Rs = 1000, 3000, and 7000 rpm, respectively. For larger d, larger dimensions of the mesh structure were produced.

Figure 2.8(d) shows the transmittance through two mesh structures of Ag ink constructed using the PS particles of d = 10 and 25 μm as a function of the wavelength in the range from 350 nm to 900 nm. The two mesh structures exhibit similar spectral behaviors but different magnitudes from each other. This is evident from the fact that the number of the mesh lines per unit area increases and the total area of the hemispherical pores decreases with decreasing the diameter of the PS particles used.

The surface nanomesh of Ag ink can be formed with high uniformity on substrate. For the quantification of the uniformity, the image J program is used. After the formation of Ag nanomesh on substrate which size is about 4 cm^2, five SEM images which are the Ag nanomesh with unit area (0.25 mm^2) is applied to image analysis. In image analysis, the standard deviation about the shape of the Ag mesh represents the defects of Ag mesh which is from the miss-alignment and missing point of colloidal particle template. The standard deviation of the surface Ag mesh is about 4 % in 10 um PS template and 3 % in 25 um PS template. Such defects in Ag mesh can decrease the performance of device by increase the resistance of Ag mesh. However, in our case, the amount of defects is so small that the Ag mesh can be applied as the network electrode. In addition, the defects are fully covered by the Ag nanoparticles that the short circuit of network electrode never be happened. Therefore, even the defects are existed, the Ag mesh as the network electrode still can be applied.

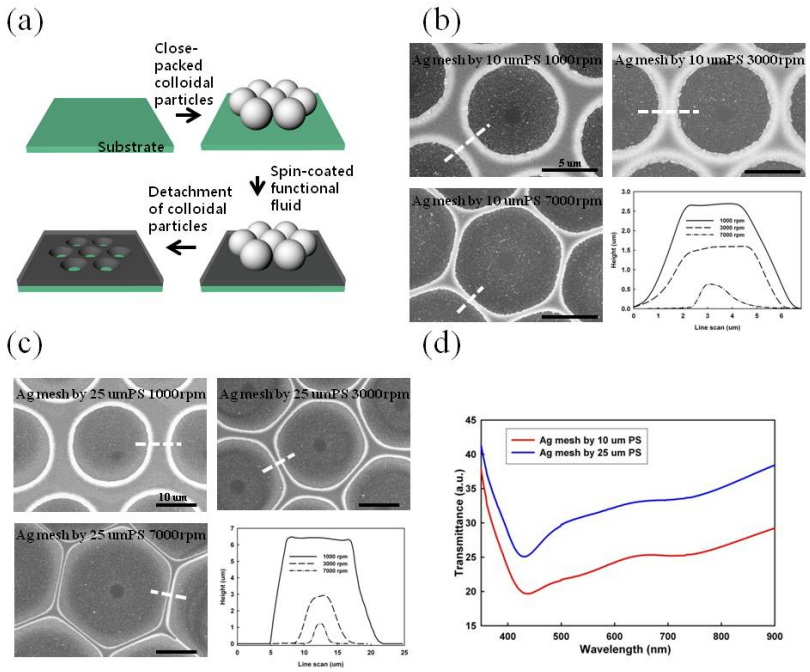

Figure 2. 8 (a) The schematic diagram of Ag mesh structure. The SEM images of the Ag mesh structures produced using the PS particles of (b) d = 10 μm and (c) d = 25 μm at three different values of Rs = 1000, 3000, and 7000 rpm. The corresponding geometrical profiles (scanned along the white dashed lines) of a single Ag mesh line having a trapezoidal cross-section were also shown. (d) The transmittance through two mesh structures of Ag ink constructed using the PS particles of d = 10 and 25 μm as a function of the wavelength.

2.4.2 Scalable nanonetwork by selective etching

Figure 2.9 shows the underlying concept of the size scalable conducting nanonetwork formation by selective etching process using GEL on Au deposited electrode. The GEL can be formed spontaneously by the liquid

bridging phenomenon on self-organized colloidal particles. Following the basic principle of liquid bridging phenomenon, the contact spot between the spontaneously formed GEL and Au electrode is smaller than the diameter of colloidal particle. Therefore, the nano-sized etching process can be achieved using the micro-sized colloidal particles. In addition, as shown in Fig. 2.8, the network formation of Au electrode can be controlled by the etching time. When the induced etching process is less than the critical time, the Au electrode cannot be formed as the network since the etching process is not enough to reach the full thickness of bottom electrode material. In the same way, the Au electrode would be fully etched by the etching process over the critical time. Therefore, for the crucial formation of conducting nanonetwork with size scalability, the etching time should be between the under etching time and over etching time. In the range of the under and over etching time, the structural property which is the line-width of conducting nanonetwork can be modulated by the etching time with the same periodicity by the diameter of colloidal particle. This means that the size of pores and the width of lines can be controlled for that can lead the various optical and electrical properties of conducting nanonetworks. With this simple and versatile method for the size scalable conducting nanonetwork, various application of optics, electronics, and opto-electronics can be established.

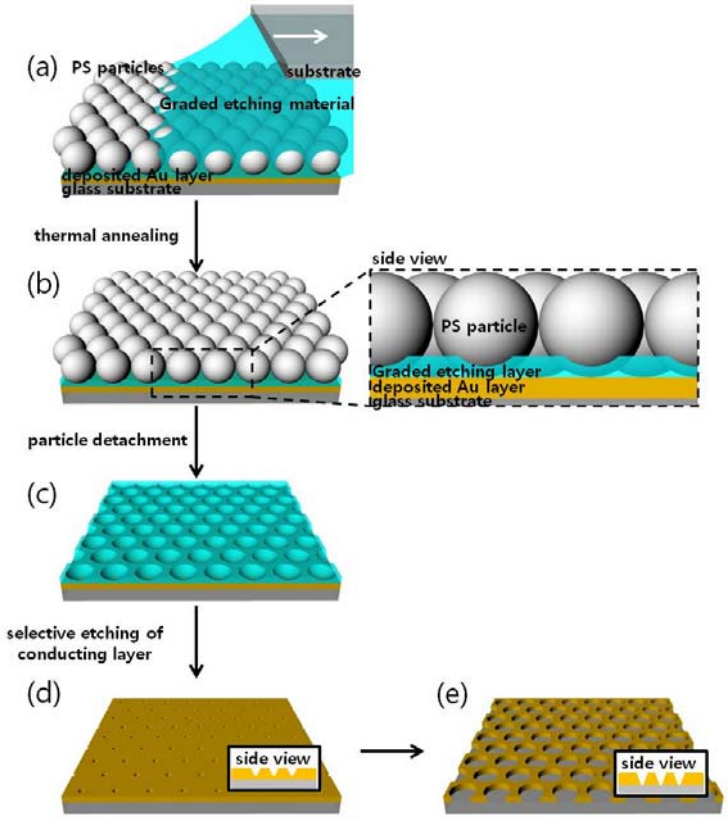

Figure 2. 9 (a) schematic diagram showing the coating process of functional fluids which is the graded etching material on self-organized colloidal particles, (b) GEL formation on self-assembled colloidal particles, (c) GEL formation after the elimination of colloidal particles, (d) conducting nanonetwork formation by selective etching process with under etching time, and (e) conducting nanonetwork formation by selective etching process with critical etching time.

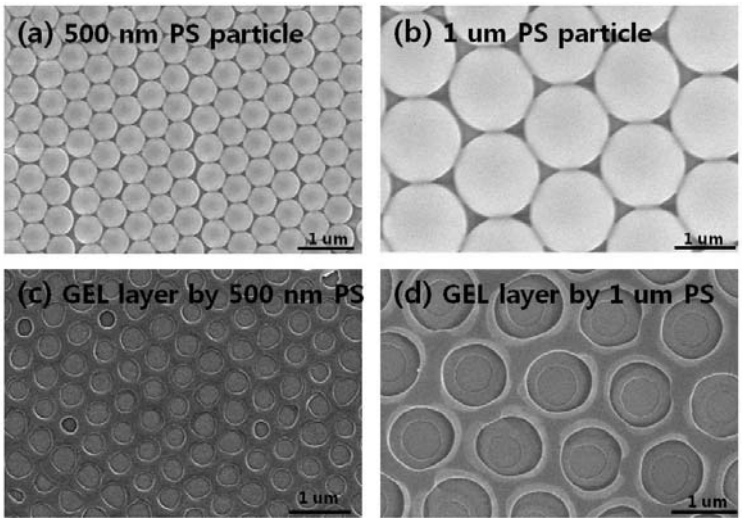

Figure 2. 10 The SEM images of the self-organized PS particles (a) 500 nm, (b) 1 um, the GEL formation of functional fluids by (c) 500 nm PS, (d) 1 um PS.

For the realization of size scalable conducting nanonetwork, first of all, the colloidal particles should be organized on substrate to induce the liquid bridging phenomenon of graded etching material, as shown in Fig. 2.9. The convective method can help to organized formation of colloidal particles which sizes are 500 nm and 1 um in diameter by simple dipping process on Au deposited electrode with UV-Ozone treatment for hydrophilic surface [52]. Since the bottom electrode can be made various kinds of metal materials, the various conducting nanonetworks can be generated by altering the deposited materials. After the thermal treatment of organized colloidal particle formation for removal of residual water contents which the colloidal particles are dispersed in, the fluorinated polymer dissolved in methoxy-nonafluorobutane (HFE-7100, 3M) in 2 wt % is coated on the self-organized colloidal particles as the graded etching material. As mentioned before,

following the basic principle of liquid bridging phenomenon, the GEL can be structured with smaller size of contact spots than the diameter of colloidal particle as depicted in Fig. 2.10. Figure 2.10(a) and (b) are the scanning electron microscope images of self-organized colloidal particles which sizes are 500 nm and 1 um in diameter on Au deposited electrode. The self-organized colloidal particles can confine the etching material in the cavities between the colloidal particles. Therefore, the etching material can be formed spontaneously as the GEL on Au electrode after the elimination of colloidal particles using toluene treatment for 10 min. Since the GEL is chemically stable, the colloidal particles which are made by poly-styrene can be dissolved by toluene. Figure 2.10(c) and (d) show the GEL on substrate formed by 500 nm and 1 um sized colloidal particles, respectively. The sizes of spots which are between the GEL and Au electrode are about 200 nm for 500 nm colloidal particle and 500 nm for 1 um colloidal particle. These smaller sizes of spots can support the smaller size of etching process in visible light range even the template of colloidal particles are micro-sized, as depicted in Fig. 2.10(c) and (d).

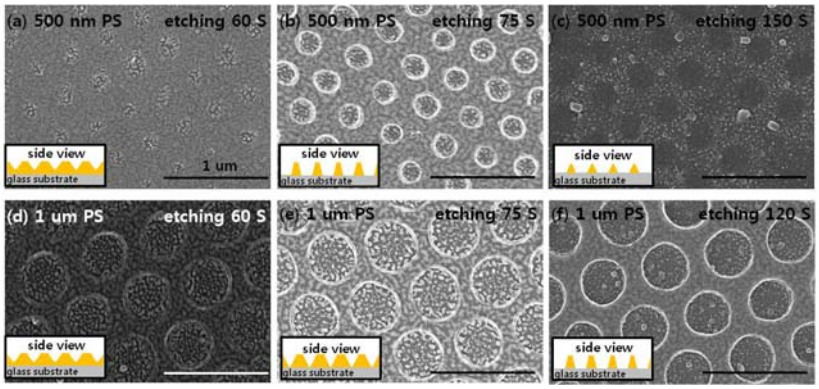

Figure 2. 11 The SEM images of selective etched Au electrode with GEL formation by 500 nm PS by various etching times (a) 60 s, (c) 75 s, (c) 150 s and GEL formation by 1 um PS by various etching times (d) 60 s, (e) 75 s, (f) 120 s, the inset images represent the side-view of Au electrode formation by selective etching process.

The formation of size scalable conducting network is made by selective etching process on GEL. The etching process is induced by O2-plasma etcher (Multiplex ICP, Surface Technology Systems) with various etching times. Since the etching process induced as the whole surface etching, the formation of GEL can help to make different etching process depending on the location. While the surface etching process cannot etch the Au electrode due to the GEL, the contacted spots between the colloidal particle and the Au electrode can be etched by the etching process since there is no GEL following the basic principle of liquid bridging. Therefore, the GEL can generate the location dependent etching process which is the selective etching process with a simple whole surface etching process. In addition, the time of etching process is one of the key factors in size scalable conducting nanonetwork formation. For the fixed thickness of Au electrode, the etching time can be calculated by the condition of etching process, for example, kinds of etching gas, pressure,

and the thickness of sacrificial layer which is the GEL. When the thickness of Au electrode is about 15 nm and the GEL formed by 500 nm PS, the critical time of etching process is about 75 sec. Figures 2.11(a), (b), and (c) show the size scalable conducting nanonetwork formation with Au electrode in 15 nm thickness by various etching time. When the etching time is not enough to fully etch the Au electrode, the cracks in the spots which are the contacted area between the colloidal particle and the Au electrode can be observed in Fig. 2.11(a). On the other hand, when the etching process is induced for more than the critical time, the Au electrode is so excessively etched that the networks are disconnected. In this situation, the Au electrode cannot be applied as the electrode due to the high resistance by disconnection. In our case, for 15 nm thickness of Au electrode with GEL using 500 nm PS, the etching process of 75 sec which is already calculated by the etching condition is the critical and practical process for the conducting nanonetwork formation as shown in Fig. 2.11(b). The spots of contacted area between the colloidal particle and the Au electrode are fully etched while the other areas are still remained by protection of GEL against the etching process. The distance between the spots is the diameter of colloidal particles naturally and the size of spots is about 200 nm since the GEL formation using 500 nm colloidal particle by liquid bridging can generate the contacted area of 200 nm sized. Moreover, when the diameter of colloidal particle increased, the size of spot and the periodicity should be altered that the various size of conducting nanonetworks can be achieved. For the formation of conducting nanonetwork using 1 um PS, the critical etching time is varied by the GEL formation, even

though the thickness of Au electrode is fixed as 15 nm. By using the bigger size of colloidal particles, the size of cavity between the colloidal particles is increased. The bigger size of cavity can make the thicker GEL that the more etching process should be induced for the fully etching of Au electrode as shown in Fig. 2.11(d), (e), and (f). When the etching time is about 60 sec, as mentioned before, the cracks in the spots the contacted areas between the colloidal particles and the Au electrode can be achieved due to the deficient etching process as shown in Fig. 2.11(d). If the induced etching time increased to 75 sec which is the critical etching time of GEL using 500 nm PS, the etched spots of Au electrode by etching process with critical time should not be fully etched due to the thicker GEL. In Fig. 2.11(e), the etching process is enough to central part of contacted spot, but the residual material has left as it goes to the edge. This means that the GEL becomes thick and the area except the contacted spots which the functional fluids cannot be positioned are covered by the thicker GEL. In the same way, when the excessively etched process is induced to the Au electrode with thicker GEL, the Au electrode should be over etched by the etching process if it follows the previous experiment which is the conducting network formation using 500 nm PS. However, in our case, the network formation by over etching process still formed as the network shape since the GEL on the Au electrode which is not the spot area can protect the Au electrode against the over etching process while the spot regions are etched. In Fig. 2.11(f), the contacted spot regions are fully etched while the other regions still maintained as the electrode formation by the over etching process. This phenomenon can be explained by

the large size of colloidal particles can generate the thicker GEL formation and the thicker GEL can protect the Au electrode more than the thinner one. Especially, following the basic principle of liquid bridging, it is not possible that the functional fluids are positioned on the contacted spots due to the existence of the colloidal particles, even though the thickness of GEL is getting bigger. For stable etching process of constructing a conducting nanonetwork formation, the thicker GEL can provide the larger range of etching time between the under and over etching times. Therefore, for construction conducting nanonetworks with various sizes of Au electrode and colloidal particles, the selective etching process should be determined by the GEL conditions.

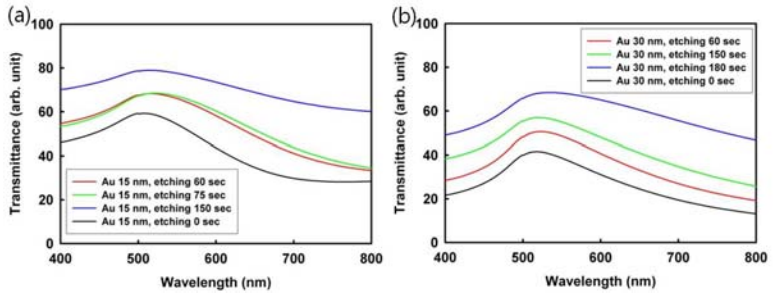

Figure 2. 12 The transmittance of scalable conducting networks made by (a) 15 nm Au electrode with various etching times and (b) 30 nm Au electrode with various etching times.

Figure 2.12(a) and (b) show the optical characteristic of our size scalable conducting nanonetworks. The optical transmittance of conducting nanonetwork with 15 nm Au using 500 nm PS is improved by increase the etching process. As the more time of etching process induced, the Au electrode is removed gradually that the more transparent electrode can be

formed. As shown in Fig. 2.12(a) and (b), the unique peak near the 500 nm wavelength can be observed by the optical property of the Au material. However, the only difference between the conducting nanonetworks with various etching times is not the shape of the curve but the magnitude of transmittance. This shows that the etching process can control the transmittance of conducting nanonetworks with single periodicity. In addition, when the thickness of Au electrode increased, it is also varied only the magnitude with the same shape of the optical transmittance. Naturally, the magnitude of optical transmittance of thicker Au electrode is smaller than that of thinner Au electrode, as depicted in Fig. 2.12. When the specific transmittance need, such optical characteristic of conducting nanonetworks can be applied to optical component since the transmittance can be manipulate by control the time of etching process.

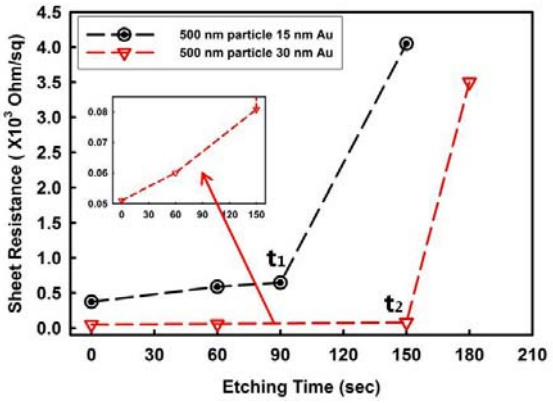

Figure 2. 13 The conductivity which is represented by the sheet resistance of scalable conducting networks with 15 nm and 30 nm Au electrode. The inset shows that the linearly increased of sheet resistance by the etching process.

The indispensable characteristic of conducting nanonetwork is the conductivity as the electrode. The conductivity of our size scalable conducting nanonetworks shows in Fig. 2.13. The sheet resistance can present the conductivity of electrode. In Fig. 2.13, in the same way of the optical transmittance of nanonetwork, the sheet resistance is increased by the inducing etching process. The etching process can remove the materials formed electrode that the cross section of electrode will be dwindled. In addition, following the basic principle of the resistance, thicker electrode, the nanonetwork with 30 nm Au in our case, has lower resistance due to the large cross section, as depicted in Fig. 3.13. Moreover, by the etching process, the sheet resistance is increased gradually and will be reached the critical point (t1 and t2 in Fig. 2.13). The critical points of the sheet resistance mean that the disconnection of the nanonetworks by the over etching process. After the critical point, the sheet resistance increased steeply due to the disconnection of nanonetworks as shown in Fig. 2.13. Therefore, before the over etching process induced, our construction method of size scalable conducting nanonetwork by selective etching process can provide the conducting nanonetworks with specific conductivity by control the time of etching process.

2.5 Nanodots Formation

The nanodots formation can be achieved by the simple lift-off process. When compared with conventional photolithography method, this method

based on the self-assembled colloidal particle can provide surface metal nanostructure with high resolution (about few hundred) and uniformity. The construction of an array of periodic nanodots of Au can be achieved with the help of a mesh structure of a sacrificial material, either AZ-1512 or EGC-1700, and a lift-off method. Thermal deposition of Au was first carried out onto the mesh structure of the sacrificial material at the pressure of 9.0×10^{-6} torr in a vacuum chamber. The nominal thickness of the Au layer was about 50 nm estimated from the thickness monitor. The mesh material was then completely removed through the lift-off process using a proper solvent, acetone for AZ-1512 and HFE-7100 for EGC-1700. As a result, the Au dots were left out only on the regions where the hemispherical pores were previously occupied in the mesh structure. As shown in the SEM images in Figs. 2.14(b) and (c), for d = 500 nm and 1 μm of the PS particles, Au dots of about 200 and 350 nm in diameter were produced using EGC-1700, respectively. For d = 10 and 25 μm, the Au dots of about 3 and 12 μm in diameter were obtained using AZ-1512 as shown in the SEM images in Figs. 2.14(d) and (e).

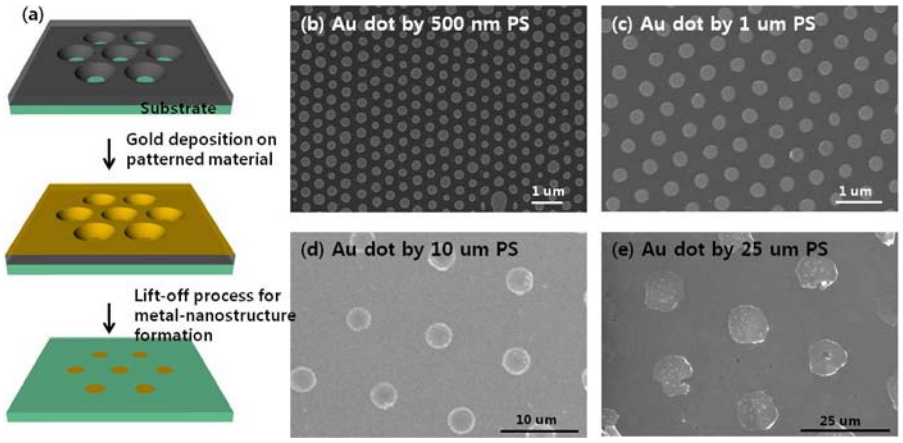

Figure 2. 14 (a) The schematic diagram of surface nano-dots formation and SEM images of the Au dots produced using the PS particles of (b) 500 nm and (c) 1 μm in diameter with the help of the mesh structure of EGC-1700. The SEM images of the Au dots produced using the PS particles of (d) 10 μm and (e) 25 μm in diameter with the help of the mesh structure of AZ-1512.

2.6 Conclusion

A generic platform for constructing periodic nanomesh structures of solidified functional fluids and nanodot arrays of conducting materials is demonstrated within the framework of liquid bridging in particle self-assemblies. The feature resolution and the pattern fidelity of the nanostructures depend primarily on the particle size, the structural arrangement in a monolayer, and the nature of liquid bridging in the particle assembly. In addition to the interfacial properties and the viscosity of the functional fluid itself, the processing conditions such as the liquid volume occupied in the pores among the nearest-neighboring particles, the coating speed, and the solvent evaporation rate were found to play crucial roles on the

geometrical shapes of the nanostructures. Moreover, the spontaneous formation of patterned sacrificial layer can induce the selective etching process to bottom electrode. Selective etching process of bottom electrode can make nano-sized pores with nano-sized periodicity. The size of pores in bottom electrode can be controlled by the inducing time of etching process. Our liquid bridging-based approach will be easily extended for other classes of functional fluids including solutions of organic semiconductors, biological substances, and color inks irrespective of the solidification. It will provide a simple and powerful tool of fabricating diverse nanodots and nanonetworks for the electrical and opto-electronic applications.

Chapter 3. Metal with Self-assembled Particles

3.1 Introduction

Metal nanostructures with dielectric materials are essential elements in various fields such as optics, photonics, and plasmonics by negative refractive index [5], interband transition [53], collective oscillation of electrons [1-3], and focusing the light by guiding effect [54]. For these unique properties of the composition of metal and dielectric material, various methods are studied. In this chapter, the two different structure of metal with self-assembled colloidal particle which are hemispherical metal cap-on-dielectric particle structure for lithographic mask by simple deposition method and surface metal nanostructure for plasmonic detection by simple detachment of self-assembled colloidal particle after the deposition process are presented. These formations of metal with self-assembled colloidal particle can provide the simple and powerful platform for opto-electric application.

3.2 Metal Nanostructures for Plasmonic Biosensor

Metal nanostructures in dielectric medium are essential elements in various fields such as optics, photonics, and plasmonics. Among them, localized surface plasmon resonance (LSPR) spectroscopy has attracted much attention for providing a simple yet efficient detection scheme through directly oscillating surface plasmon without a phase matching process needed for the conventional SPR spectroscopy [55]. Moreover, the LSPR with

uniform metal nanostructures provides an ultra-high sensitivity due to the collective oscillations of surface plasmon at each nanostructure. For constructing metal nanostructures, various methods including focused ion beam [32], electron beam lithography [17], and random placement of metal nanoparticles [56, 57] have been used. However, these methods have some weaknesses either in the mass production or long-term stability of the physisorbed nanoparticles with random distribution that could be an obstacle to develop cost effective and highly accurate LSPR biosensors. In addition, for practical application of biosensing devices, it is important to detect the protein binding event under the real cell membrane environment since the biomaterials are very sensitive for the environment [58]. Since the cell membrane environment is the aquatic environment, the surface nanostructure should be formed strongly on substrate. Therefore, metal nanostructure with a regular size, shape and with a stable environment is a prerequisite for a highly sensitive and accurate LSPR biosensor for detecting biomolecular species

3.2.1 Theoretical analysis

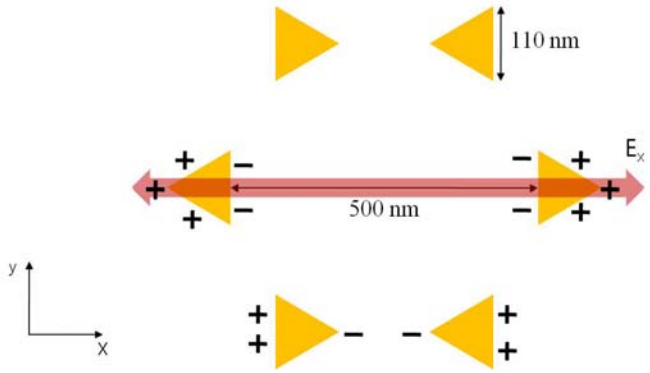

Figure 3. 1 Simulation condition with finite element method.

The Comsol Multiphysic (Altsoft co.) can provide the collective oscillation of electrons by the incident light as varying the shift of peak wavelength. The finite element method can solve the Maxwell solution in the optical structure. For absorption, transmittance, and reflectance of the light, the surface nanostructures are divided as the unit cell and set the periodic boundary condition. In this situation, the incident light with transverse magnetic mode which has the magnetic field in y direction is applied. For accurate response, every direction of polarized light should be calculated. However, such method is not available that the input light which polarized direction is x-direction is applied. Such difference between simulation and real experiment can generate the error in simulation since the incident light with unpolarized light is employed in real experiment.

In simulation, the refractive indices of water, lipid membrane, and protein are 1.43, 2, and 1.6, respectively. In addition, the structural condition of surface nanostructure is set according to the experimental condition.

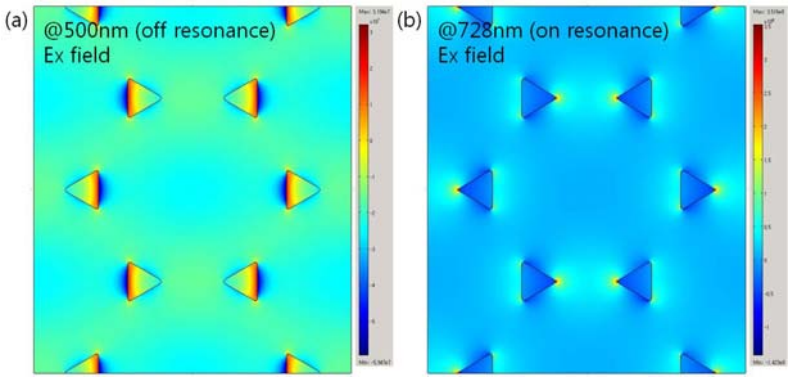

Figure 3. 2 Simulation result of plasmonic resonance in surface metal nanostructure with various wavelength of incident light.

As shown in Fig. 3.2, the electric field by incident light is generated. In 728 nm wavelength which is the resonance wavelength, the intensity of electric field is maximized in tip of the structure. In 500 nm wavelength which is not the resonance wavelength, the intensity of electric field is smaller than the resonance state about 10%. Therefore, the electric field with strong intensity can induce the absorption of incident light that the plasmonic signal can be generated. Using such basic phenomenon, the plasmonic biosensor can be achieved with various dielectric constants surrounding the metal nanostructures.

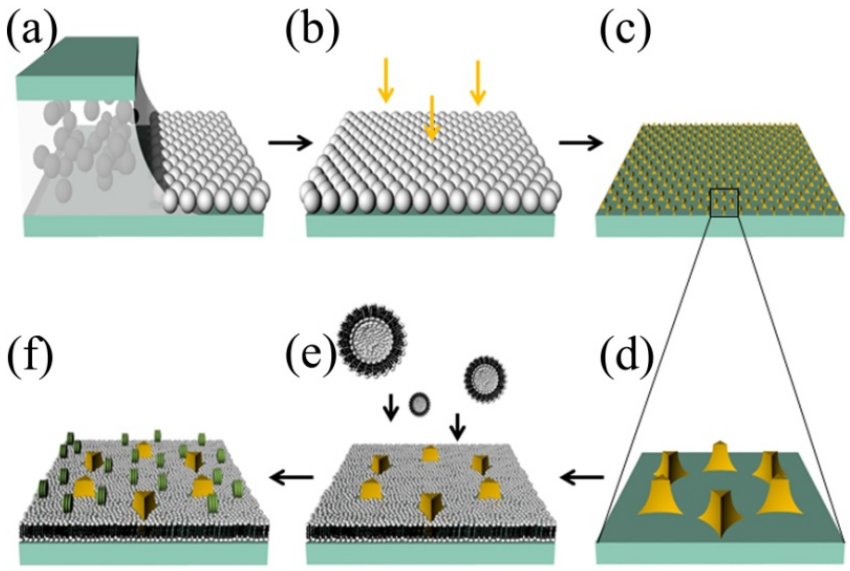

Figure 3. 3 Schematic diagrams of the NSL, SLBs formation and protein binding event.

3.2.2 Nanosphere lithography for surface nanostructure

For the construction of suface metal nanostructure, the substrate was cleaned with a piranha solution (3:1 (v/v) H2SO4: H2O2) at 80 ℃ for 20 min, followed by sonication in deionized (DI) water for 10 min. Through the convective method , polystyrene (PS, Duke Science) spheres of 300 nm and 500 nm in diameter were arranged into a close-packed monolayer formation on the substrate as shown in Fig. 3.2(a). The gold layer was deposited about 50 nm using a thermal evaporator. After the detachment of nanoparticles through the sonication in DI water for 10 min, the periodic gold nanostructures deposited through the open space between particles were remained on the substrate with triangular shape and nano-ranged periodicity Figs. 5.3(a) and (b) show SEM (S-4800, Hitachi) images of the gold

nanostructures which are made by 300 and 500 nm colloidal particles. The sizes of major axis are 70 nm and 116 nm by 300 nm and 500 nm particle, respectively. In addition, the gold was deposited for stable detection in water, since gold is more inert than others in solvent.

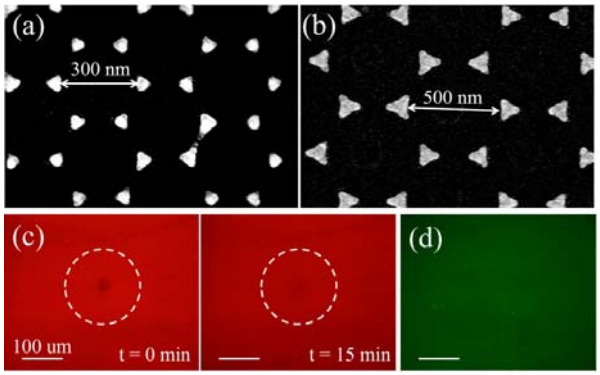

Figure 3. 4 SEM image of gold nanostructure (a) by 300nm PS, (b) by 500nm PS, and the fluorescence microscope images of (c) the SLBs formation with fluidity, (d) protein binding event.

3.2.3 Supported lipid bilayers for cell membrane environment

The substrate with gold nanostructures was treated by ultraviolet-ozone that a hydrophilic surface in dielectric regions is suitable for the vesicular adsorption and rupture leading to the SLBs formation. The mixture of lipids with 1,2-dioleoyl-sn-glycero-3-phophocholine (DOPC, Avanti Polar Lipids) and 1,2-dipalmitoyl-sn- glycero-3-phosphoethanolamine-N-(cap biotinyl), sodium salt (biotin-DPPE, Avanti Polar Lipids) was used to produce the small unilamellar vesicles (SUVs). For imaging the SLBs, a red fluorescent dye labeled lipid, 1,2-dihexadecanoyl-sn-glycero- 3-phosphoethanolamine (Texas Red-DHPE, Molecular Probes) was mixed with DOPC at 1 mol %. The vesicle solutions were prepared by hydration of dried lipids in Tris buffer (100

mM NaCl, 10 mM Tris at pH 8.0) with a total lipid concentration of 0.2 mg/ml. After the hydration, the SUVs were obtained by the extrusion method (Mini-Extruder, Avanti) with 20 filtering processes through a 50 nm filter. The SLBs was formed by the fusion of SUVs on the substrate for 10 minutes as shown in Fig. 3. 2(e). The fluorescent dyes were monitored using an epifluorescence microscopy (Eclipse E600-POL, Nikon). In addition, the SLBs doped with biotin-DPPE was incubated in a PBS (phosphate buffer saline at pH 7.2) solution containing streptavidin or streptavidin conjugated with Alexa Fluor 488 (Molecular Probes) at 5 g/ml for 30 min as depicted in Fig. 3.2(f). In addition, for the plasmonic signal, the visible-IR spectrometer (Jasco-V530) was used. Moreover, for preventing fluorescent dye effect, lipid membranes and proteins without any fluorescence dye are used. Figure 3.3(c) shows fluorescence recovery after photobleaching (FRAP). FRAP show the fluidity of lipid membrane and the recovery of bleached lipid over time can be observed. Thus, the stable and well-formed of lipid membrane can be confirmed by its fluidity. Moreover, Figure 3.3(d) shows specific binding of protein to ligand by fluorescence microscope. Since ligands are uniformly distributed with SLBs, the proteins can be bonded uniformly to ligand on substrate.

3.2.4 Plasmonic detection of protein binding event

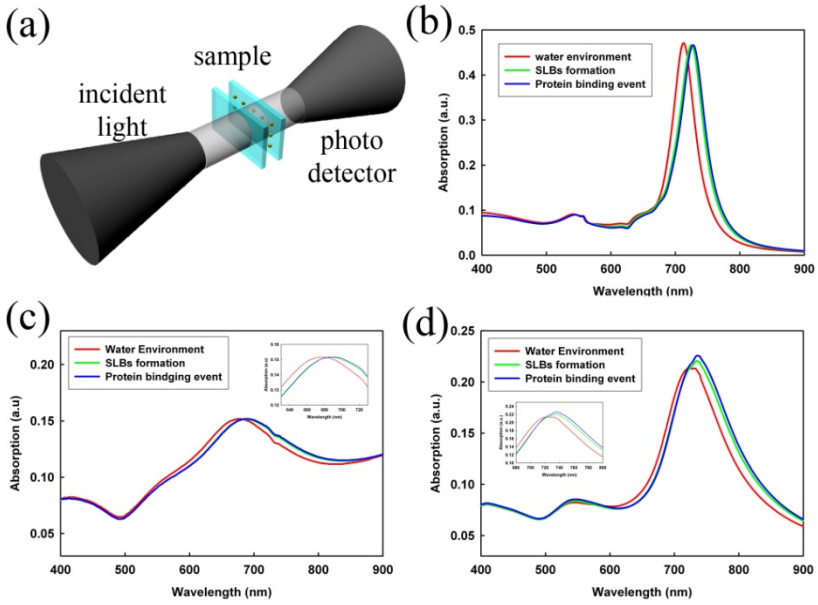

Figure 3. 5 (a) schematic of optical measurement, and absorption spectrum by SLBs formation and protein binding event (b) simulation result of 500nm PS, (c) experimental result of 300 nm PS, and (d) experiment result of 500 nm PS.

Now, the plasmonic responses of surface gold nanostructures by the formation of SLBs and protein binding event are examined through the simulation and experiment. The measurement set-up is shown in Fig. 3.4(a). The input light passes though the sample and the photodetector can get the absorption signal. Figure 3.4(b) shows the simulation result of absorption spectrum with 500 nm PS template. The absorption peak wavelength is 713 nm in water. After the formation of SLBs, the peak wavelength is shifted about 12 nm and again 3 nm shifted from 725 nm to 728 nm by protein binding. These shifts of peak wavelength show that the dielectric constant changed by biological activities. These phenomena also can be seen in

experimental result, as depicted in Fig. 3.4(d). There are some differences between the simulation and experimental result. However, the peak wavelength and variation are similar since the peak wavelengths in experimental result are 723 nm in water environment, 734 nm in SLBs formation, and 736 nm in protein binding event. These similar values of peak wavelength and the amount of peak shift show that the simulation result can predict the experimental result and fit well for the realization of plasmonics biosensor. Another case which is surface gold nanostructure made by 300 nm colloidal particle are shown in Fig. 3.4(c). When the substrate is filled with water, the peak wavelength is 677 nm. Then it changes 11 nm by the SLBs formation and again 2 nm shifted by protein binding event. This result is bigger than established result due to the uniform size and regular shape of metal nanostructures [60]. In addition, due to the metal nanostructures with regular size and shape, the mean free path of electron is fixed. Such a restriction of mean free path can produce the not only single peak but also sharp peak of our absorption spectrum [61]. Moreover, the periodicity of metal nanostructure can prevent the random coupling effect which can be decrease the resolution and accuracy of biosensor by broadening the curves. For LSPR biosensor that the peak shift is within a few nanometer ranges, it can be a huge error for biosensing even if a small noise existed. Furthermore, the difference of LSPR phenomena by inter-particle distance variation can be observed. When the inter-particle distance increase, the peak is red-shifted since the electron's restoring force is weakened and the width of curve is narrowed due to large mean free path without any random coupling effect.

Therefore, the structural properties of metal nanostructure can be modulated by altering the size of colloidal particle for accurate plasmonic biosensor.

3.3 Metal on Spherical Particles for Lithographic Mask

The photolithography with structured mask has attracted a great deal of attentions due to the smaller feature size of photoresistor [14, 15]. The light passed through the structured mask can be manipulated to focus the beam spot and the focused beam spot can provide the smaller feature size. One of the crucial challenges for the construction of the structured mask is the selectively passing the light. Using the transparent material to guide the light in small aperture, additional pre-patterned metal layer can prohibit the light transmission. Therefore, small size of feature can be achieved. However, this method needs the additional process to make small apertures for transmission of light and such small apertures are hard to make. In order to avoid such smaller aperture formation, there is a phenomenon of focusing light by transparent spherical structures. When the light passed through the spherical shaped structure, the light is focused due to the different refractive index between the air and structure with spherical shaped. Though this phenomenon can focus the light in small features, it is hard to restrict the penetrated light in non-focused region.

3.3.1 Hemispherical metal cap-on dielectric particle

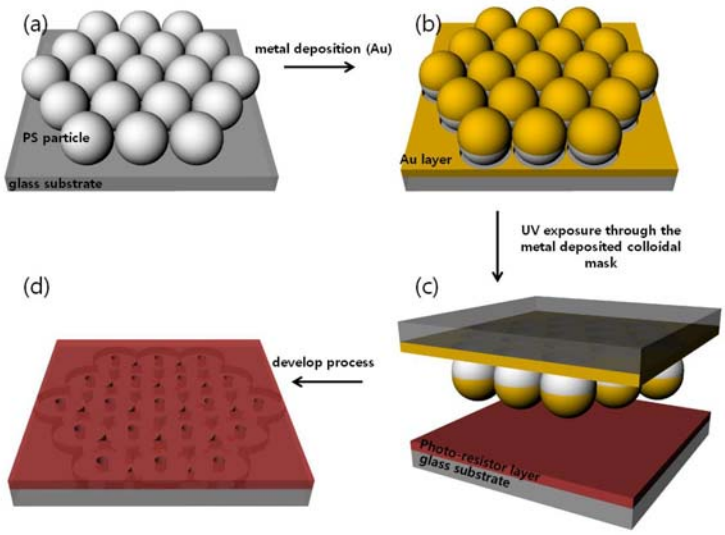

Figure 3. 6 Schematic diagram of optical field focusing effect in hemispherical metal cap-on-dielectric particles for lithographic microstructures.

Figure 3.5 shows the schematic diagram of optical focusing effect using metal deposited colloidal particle mask. The AZ-1512 which is the photoresistor is coated on substrate with 3000 rpm for 30 sec. After the pre-baking process in 90oC for 1 min, the AZ-1512 coated substrate is exposed by the UV light for photosensitization of AZ-1512. By removal process of unexposed AZ-1512 using developer (AZ-300, AZ Electronic Materials), the feature size of photosensitization can be observed by SEM.

The colloidal particles used in this study were PS particles sized 10 um, 25 um, and 100 um in diameter as shown in Fig. 3.6. They were dispersed in water with a detergent (surfactant) which stabilizes the colloidal dispersion by preventing the particles from aggregation. The detergent in water should be

removed for constructing spherical PS structures on a substrate. After the colloid was centrifuged at 10000 rpm for 10 min for separation of colloidal particles, the detergent was removed with water. For critical concentration of colloidal particles with colloidal dispersion in water, DI water was filled for 3 weight percent of colloidal particles, and ultra-sonication was subsequently carried out for 10 min. The colloidal particles in DI water were drop-coated on substrate as shown in Fig.3.6. Before the metal deposition on colloidal particle structure, the substrate with colloidal particles should be baked at 65°C for 120 min for elimination of the residual water contents between the colloidal particles. The metal layer on colloidal particles is deposited with various thicknesses such as 20 nm, 40 nm, 80 nm, 100 nm, and 200 nm using thermal evaporator.

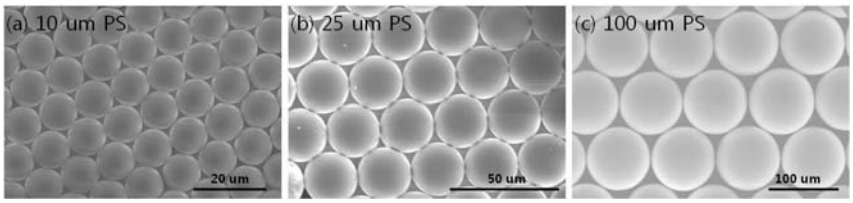

Figure 3. 7 Close-packed monolayer formation of colloidal particles which size are (a) 10 um, (b) 25 um, and (c) 100 um in diameter.

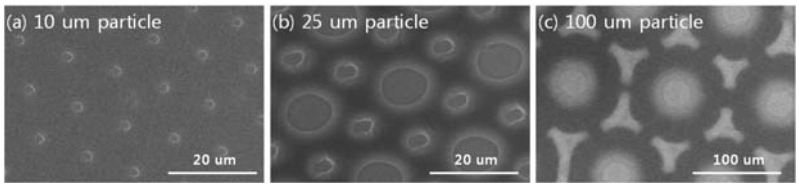

Figure 3. 8 Optical field focusing effect using various size of colloidal particles with Au layer of 20 nm.

3.3.2 Light focusing effect and metal thickness dependency

Figure 3.7 show the optical field focusing effect in hemispherical metal cap-on-dielectric particles for lithographic microstructures. Though the induced light can expose the whole area of AZ-1512 coated substrate, the focusing effect can regulate the pathway of light that the focused light can sensitize the photoresistor selectively. The non-focused region cannot be exposed by the penetrated light due to the 20 nm deposited metal layer. The spot size of photosensitization is smaller than the diameter of colloidal particles. Therefore, this method can generate smaller features with simple process.

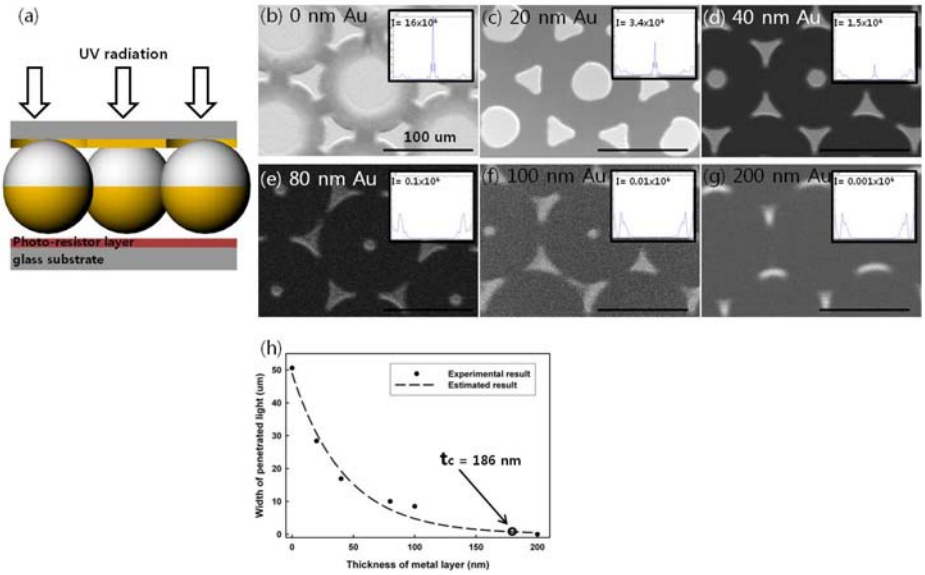

Figure 3. 9 Optical field focusing effect using various thickness of Au layer

In addition, using various thicknesses of metal layer, the feature size can be modulated. By fixed size of colloidal particle, the amount of focusing is also fixed. However, the feature size of penetrated light can be controlled by employing the different thickness of metal layer, since the magnitude of penetrated light should be Gaussian distribution. Therefore, the feature size of penetrated light is decreased by the increase of metal thickness as shown in Fig.3.8. Moreover, the feature size of penetrated light is extremely reduce by the focusing and blocking effect since the feature size is a few micrometer even the size of colloidal particle is 100 um. The inset images show the simulation result of penetrated light intensity in various size of colloidal particle mask. Furthermore, using the experimental result, the critical thickness of metal layer which can perfectly prevent the penetration of light can be predicted. Since the resolution of feature is limited by the wavelength of exposed light, when the metal thickness is about 186 nm, the exposed light cannot penetrate the colloidal mask.

3.3.3 Reversal pattern formation

Figure 3.9 shows the reversal pattern formation using the metal deposited colloidal particle mask. The reversal pattern formation can be produced by different processes which are the lift-off process and etching process. One case, using the lift-off process, thermally deposited metal layer on photosensitized photoresistor after the exposed light through the metal deposited colloidal particle mask. The Al microstructure can be formed on substrate by elimination of photoresistor using acetone treatment for 1 min.

The other case, using the etching process, the photoresistor is coated on metal deposited substrate. After the exposed light through the metal deposited colloidal particle mask, the etching process is induced to patterned photoresistor substrate. By the etching process, the electrode is etched selectively due to the patterned photoresistor. This method can make the micronetwork electrode.

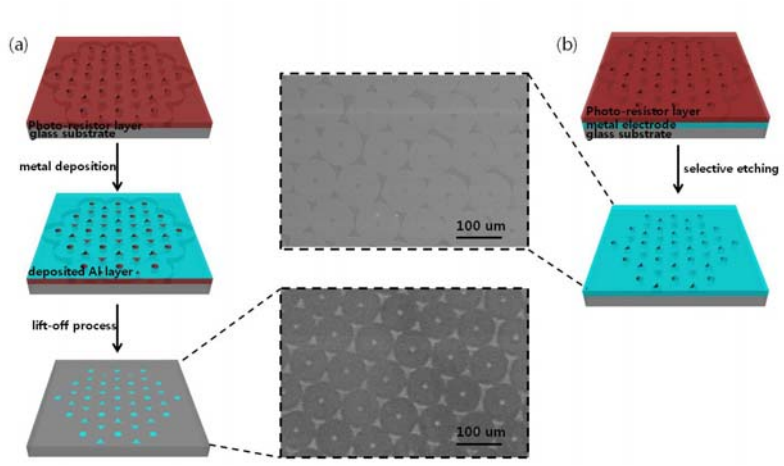

Figure 3. 10 Reversal pattern formation.

3.4 Conclusion

The two different structure of metal with self-assembled colloidal particle which are hemispherical metal cap-on-dielectric particle structure for lithographic mask by simple deposition method and surface metal nanostructure for plasmonic detection by simple detachment of self-assembled colloidal particle after the deposition process are presented. The plasmonic biosensor with uniform and regular formation of metal nanostructures for the detection of the protein binding on SLBs can provide the accurate biosensing

application. The gold nanostructures by NSL using 300 nm and 500 nm PS particles are provided and it generate the accurate plasmonic signal for detection of dielectric changes by biomaterials. This approach of biosensor which can detect under membrane formation can be a new platform for understanding the biological activities that occur in cell membrane environment. In addition, the construction method of nano- to micro-structure on the substrate by light focusing effect using colloidal particles with various sizes and period is presented. Since the nano- to micro-particles can focus the light because of the colloidal particle's shape spontaneously, the narrower beam spot of UV light in photolithography can be generated. A layer of colloidal particles was prepared on the glass substrate by drop coating a solution of PS particles. The substrate with PS particles thermally deposited with gold about 20 nm and 80 nm for application of light focusing mask in photolithography. Then, photo-resist deposited substrate was exposed the UV light through the light focusing mask. The UV light can pass the gold layers with colloidal particles by the light focusing effect. However, the gold layers without colloidal particles can block the UV light. Therefore, various dimensions and period nano- to micro-structures can be generated by control the size of colloidal particles. This method can provide a variable platform for studying nanostructure based-devices.

Chapter 4. Nanostructures for Interaction with Nanomaterials

4.1 Introduction

Recently, nanotechnology has been paid much attention for developing new types of devices in diverse fields, such as optics [62], electronics [63], fluidics [64], and biochemistry [65]. Particularly, it plays a critical role in manipulating interfacial interactions of various functional molecules, for example, liquid crystals (LCs) [66], conducting polymers [67], and biomolecules [68] at a molecular level or on a nanometer scale. A number of surface nanostructures have been constructed by taking either conventional top-down approaches such as a photolithography [14] and an e-beam lithography [16] or bottom-up approaches that include a soft lithography [18], a stamping technique [21], and a self-assembly method [20-22]. Among them, the self-assembly method is promising due to the merits of high throughput, large area, low cost, and high resolution. However, it encounters with the problem of mechanical stability due to relatively weak adhesion of colloidal particles on a substrate. For instance, template-assisted self-assembling [32] and micro-contact printing [35] are known to be useful for producing regular patterns of colloidal particles but they suffer from low stability. Moreover, once the colloidal particles are assembled to form certain structures on the

substrate, it is very difficult to modify the geometrical dimensions (width, length, and height) of the structures.

In this chapter, a simple and powerful method of constructing the surface nanotopography on a basis of the colloidal particles by thermal fixation is presented. This colloidal particle-based approach together with thermal fixation provides the surface nanotopography with size-scalable nanostructures for controlling interfacial structural orders of the functional molecules in a variety of electro-optic devices. The experimental results for the structural changes of the particles by thermal treatment are in good agreement with the calculations in a simple model of the constant-volume. It is found that the LC alignment on the hemispherical nanostructures increases the symmetry of the electro-optic properties of the LC devices.

4.2 Thermal Fixation

The colloidal particles used in this study were PS particles (1 μm in diameter, Duke Science Inc.) dispersed in water with a detergent (surfactant) which stabilizes the colloidal dispersion by preventing the particles from aggregation. For constructing pure PS nanostructures on a substrate, water with the surfactant should be replaced by deionized (DI) water prior to spin-coating of the colloidal particles on the substrate. After the colloid was centrifuged at 10000 rpm for 10 min for precipitation of the particles, water with the surfactant was removed, DI water was then filled, and ultra-sonication was subsequently carried out for 10 min to acquire colloidal dispersion in DI water. The colloidal particles in DI water were spin-coated on

an indium-tin-oxide coated glass substrate at 3000 rpm for 30 sec. The number density of the PS particles per area (mm2) was determined using ImageJ program (National Institutes of Health). In order to examine the thermal fixation and the structural changes of the PS particles, the substrate coated with the colloidal PS particles was heated at 200°C above the glass transition temperature of the PS (about 93 °C) [69] for several different duration times (from 1 min to 240 min). The topographic changes of the PS particles were observed using an atomic force microscope (AFM, XE-100, Park System Co.) and a scanning electron microscope.

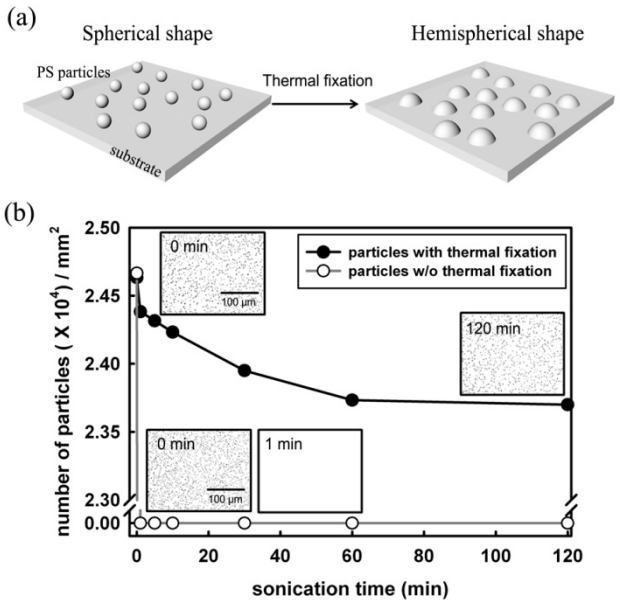

Figure 4. 1 (a) schematic diagram showing the structural changes of the PS colloidal particles by thermal fixation and (b) the experimental results for the detachment of the PS particles under ultra-sonication demonstrating the mechanical stability of the hemisph hemispherical PS nanostructures.

The underlying concept of the surface nanotopography based on colloidal particles is depicted in Fig. 4.1 where the structural changes and the mechanical stability of the PS particles are achieved by thermal fixation. The PS particles are first dispersed in a random monolayer on a glass substrate by spin-coating and they undergo the structural transformation into hemispherical nanostructures under the thermal treatment as shown in Fig. 4.1(a). The spin-coated PS particles have very weak adhesion but the hemispherical PS nanostructures formed by thermal fixation have high mechanical stability. Figure 4.1(b) shows the experimental results for the detachment under ultra-sonication demonstrating the mechanical stability of the spin-coated PS particles and that of the hemispherical PS nanostructures formed by thermal fixation at 200°C for 120 min. The number density of the PS particles remained on the substrate was measured as a function of the ultra-sonication time. The insets in Fig. 4.1(b) show the contrast-enhanced images converted from the optical microscopic images using an image analysis program. Clearly, the spin-coated PS particles without thermal fixation were fully detached from the substrate in 1 min under ultra-sonication. However, the PS nanostructures formed by thermal fixation were mostly remained (more than 96 %) on the substrate during ultra-sonication for 120 min in time. This implies that thermal fixation of colloidal particles is a powerful tool of constructing the surface nanotopography with high mechanical stability.

Let us describe the size-scalability of the surface nanotopography based on the colloidal particles. In our case, such scalability can be achieved by simply varying the time of the thermal treatment for the structural changes of the PS

particles. Figure 4.2(a) shows the SEM images demonstrating the structural changes of the PS particles by the thermal treatment at 200°C for 1 min and 60 min. Due to the softening17 of the PS particles at 200°C, the height of the individual PS structure decreases while the contact area (or the width) increases with increasing the time of the thermal treatment. More specifically, assuming that the volume of the PS particle remains constant in a first-order approximation, one can easily estimate the height h of the surface structure from the radius r of a virtual sphere whose portion is equal to the original volume of the PS sphere without the thermal treatment as shown in Fig. 4(b). In a simple model of the constant-volume, the radius r is given by

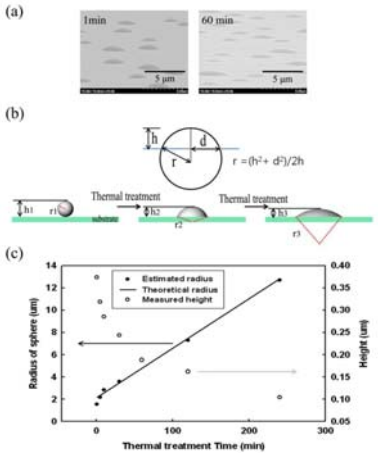

Figure 4. 2 (a) The SEM images demonstrating the structural changes of the PS particles by the thermal treatment in time, (b) a schematic diagram showing the radius change of a virtual sphere in a simple model of the constant-volume under the thermal treatment, and (c) the measured average height of the hemispherical PS nanostructures and the radius of a virtual sphere estimated from the height. The solid line represents the theoretical values of the radius calculated in the constant-volume model.

$$r = (h^2 + d^2)/2h, \quad (1)$$

where h and d denote the height and one half of the width representing the area of the surface structure in contact with the substrate, respectively. Under the thermal treatment in time, the height h (or the corresponding r) will evolve as h_1, h_2, and h_3 (or r_1, r_2, and r_3). In Fig. 4.2(c), the measured average height of the PS structures and the estimated radius in the constant-volume model were shown as a function of the thermal treatment time. It was found that the average height of the PS structures is in the range from 1 μm (the original diameter of the PS sphere) to 104 nm under the thermal treatment from 0 to 240 min. The solid line represents the estimated values of the radius from the measured values of the average height of the surface nanostructures. In the constant-volume model, the surface nanotopography based on the colloidal particles will be easily tailored for a variety of device applications of functional molecules including the LCs through the topographic control of interfacial structural orders.

4.3 Liquid Crystal Display application

The ITO glass substrate with surface nanostructures of the PS particles was used as one of two substrates of the LC cell. No surface nanostructures were formed on the other to investigate the symmetry of the EO properties associated with the surface nanotopography. Polyimide (PI) materials of AL00010 (Japan Synthetic Rubber Co.) and RN-1199A (Nissan Chemical

Industries, Ltd.) were used for the homeotropic (HT) LC alignment and the homogeneous (HG) LC alignment, respectively. The alignment layers were produced on the substrates by spin-coating at 3000 rpm for 30 sec and subsequently baked at 65°C for 120 min. Note that the baking temperature of the PIs was below the glass transition temperature of the PS so as to avoid any topographic change of the PS during baking. All the substrates with the alignment layers were rubbed unidirectionally to define the easy axis of the LC molecules for the uniform alignment. For the purpose of the observation of the microscopic molecular orientation on the surface nanostructures in two different LC configurations, two types of the LC cells where the rubbing directions on the top and bottom substrates were anti-parallel to each other in the HT LC cell while they were mutually perpendicular in the 90° twisted-nematic (TN) LC were prepared. The cell gap of each LC cell was maintained using spacers of beads. The HT LC cell and the TN LC cell were 7 μm and 4 μm thick, respectively. The nematic LCs, one with negative dielectric anisotropy (MJ961213, Merck Ltd.) for the HT LC cell and the other with positive dielectric anisotropy (ZLI-2293, Merck Ltd.) for the TN LC cell, were filled into the cells by capillary action. Microscopic textures of the LCs were observed with a polarizing optical microscope (Optiphot II-pol, Nikon). The EO properties of the LC cell were measured using a photodiode in conjunction with a digitizing oscilloscope (Wave Runner 6030, LeCroy). The dynamic response of the LC cell was measured using a square wave voltage

of 4 V at 1 kHz. A light source was a He-Ne laser with the wavelength of 632.8 nm. A spatial photometer (EZ-contrast 160 R, ELDIM) was used to measure the iso-contrast map which represents the symmetry of the EO properties as well as the viewing angle characteristic of the LC cell. All the measurements were carried out at room temperature.

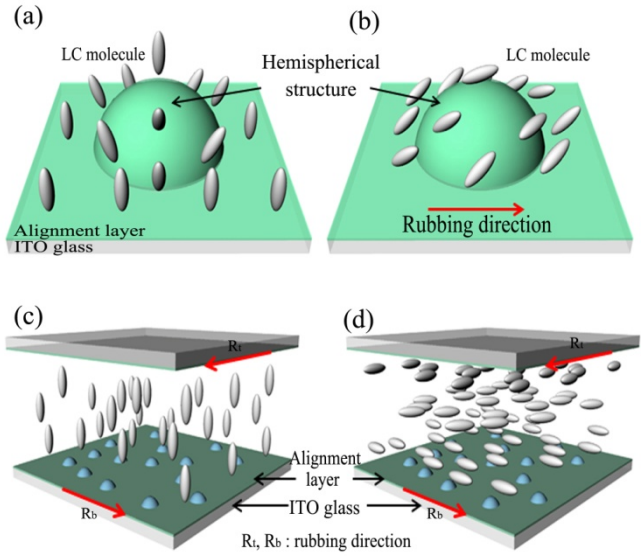

Figure 4. 3 Schematic diagrams of the LC alignment with (a) the hemispherical symmetry on the surface nanostructure in the HT geometry without the rubbing process and (b) the partially uniaxial symmetry on the surface nanostructure along the rubbing direction. Device configurations of (c) a HT LC cell and (d) a TN LC cell assembled with the bottom substrate with the hemispherical nanostructures and the top substrate without them. Two rubbing directions are represented by Rt (on the top surface) and Rb (on the bottom surface).

The Figs. 4.3 show how the surface nanotopography of the PS structures influences the LC alignment and the resultant EO properties of two types of the LC cells, one of which is the HT LC cell and the other the TN LC cell. Figures 4.3(a) and 4.3(b) show the LC alignment with the hemispherical symmetry on the surface nanostructure in the HT geometry and that with the partially uniaxial symmetry in the HG geometry, respectively. The surface pretilt generated during the rubbing process is typically a few degrees depending on the nature of the alignment layer [70]. Thus, the symmetry-breaking effect by the surface pretilt is relatively small compared to that by the surface nanostructures. A HT LC cell and a TN LC cell assembled with the bottom substrate with the surface nanostructures and the top substrate without them are depicted in Figs. 4.3(c) and 4.3(d), respectively. Two rubbing directions are represented by Rt (on the top surface) and Rb (on the bottom surface). Under no applied voltage, the HT LC cell is in the normally dark state while the TN LC cell is in the normally white state under crossed polarizers. In the absence of an external field, the local alignment of the LC molecules in the HT cell possesses the nearly hemispherical symmetry with some directional order by the rubbing process while that in the TN cell has the uniaxial symmetry along the rubbing direction on the nanostructure surfaces. Macroscopically, this will be reflected in the symmetry of the EO properties of each LC cell.

In the two types of the LC cells studied, the number density of the PS particles on the bottom substrate was about 2.46×10^4 / mm^2. The surface structures produced by the thermal treatment for 120 min were 162 nm high and 3 μm wide. Figures 4.4(a) and 4.4(b) show the microscopic LC (MJ961213) textures observed under crossed polarizers at the applied voltages of 0 and 7 V in the HT LC cell, respectively. In the absence of an applied voltage, a completely dark state was obtained, meaning that the surface pretilt has no appreciable effect in the HT geometry. At 7 V, due to the negative dielectric anisotropy, the LC molecules were reoriented toward the substrate plane along the rubbing direction from the initial direction normal to the substrate, and a bright state was accordingly obtained. For the TN LC cell, the microscopic LC (ZLI-2293) textures at 0 and 7 V under crossed polarizers are shown in Figs. 4.4(c) and 4.4(d), respectively. Line defects observed in the TN LC cell are attributed to the mechanical scratches involved incidentally during the rubbing process and they would be avoided by changing the rubbing strength and/or the rubbing cloth. Under no applied voltage, the LC molecules were initially twisted in the TN configuration. In this case, due to the wave-guiding effect, the TN LC cell was in a bright state. At 7 V, the LC molecules were reoriented toward the direction normal to the substrate because of the positive dielectric anisotropy, and a dark state was produced. It may be noted that the EO properties of the two types of the LC cells (the HT and TN LC cells) are approximately reciprocal from the viewpoint of the LC distortions associated with the dielectric anisotropy.

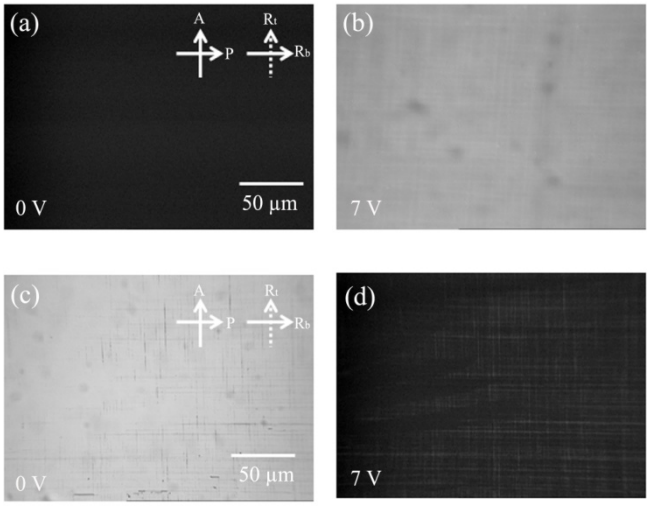

Figure 4. 4 Microscopic LC textures observed under crossed polarizers; the LC textures at (a) 0 V in the HT LC cell, (b) 7 V in the HT LC cell, at (c) 0 V in the TN LC cell, and (d) 7 V in the TN LC cell. The analyzer and the polarizer are denoted by A and P, respectively. Two rubbing directions are represented by Rt (on the top surface) and Rb (on the bottom surface).

Figure 4.5(a) shows the normalized EO transmittance of the HT LC cell with the surface nanostructures together with that without the surface nanostructures as a function of the applied voltage. The dynamic response of the HT LC cell to a square wave voltage of 4 V at 1 kHz was shown in Fig. 4.5(b). In the two HT LC cells, the EO transmittance was slightly different but the threshold voltage (about 2.5 V) remains nearly same. For the HT LC cell with no surface nanostructures, the rising and falling times were about 80 msec and 42 msec, respectively. They were much reduced to be about 67 msec and 18 msec for the HT LC cell with the surface nanostructures. Such difference between the two HT LCs results primarily from the energy cost

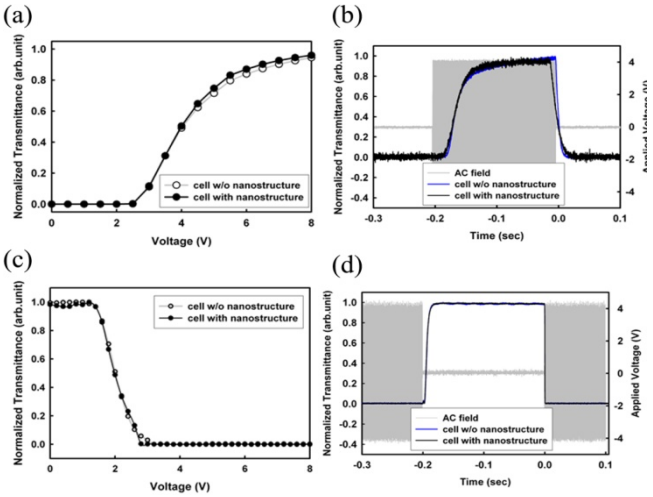

Figure 4. 5 (a) The normalized electro-optic transmittance as a function of the applied voltage and (b) the dynamic response of the HT LC cell. (c) The normalized electro-optic transmittance as a function of the applied voltage and (d) the dynamic response of the TN LC cell. The dynamic response of the LC cell was measured using a square wave voltage of 4 V at 1 kHz.

associated with the elastic distortions of the hemispherical alignment of the LC molecules on and around the surface nanostructures. Figures 4.5(c) and 4.5(d) show the normalized EO transmittance and the dynamic response for the TN LC cells with and without the surface nanostructures, respectively. The threshold voltage (about 1.5 V) and the EO transmission were found to be essentially same in the two TN LC cells. The rising times for the TN LC cells with and without the surface nanostructures were about 6.8 msec and 1 msec, respectively. The falling times for the two TN cells were the same as 1 msec. The results for the two TN LC cells imply that the elastic distortions of the LC

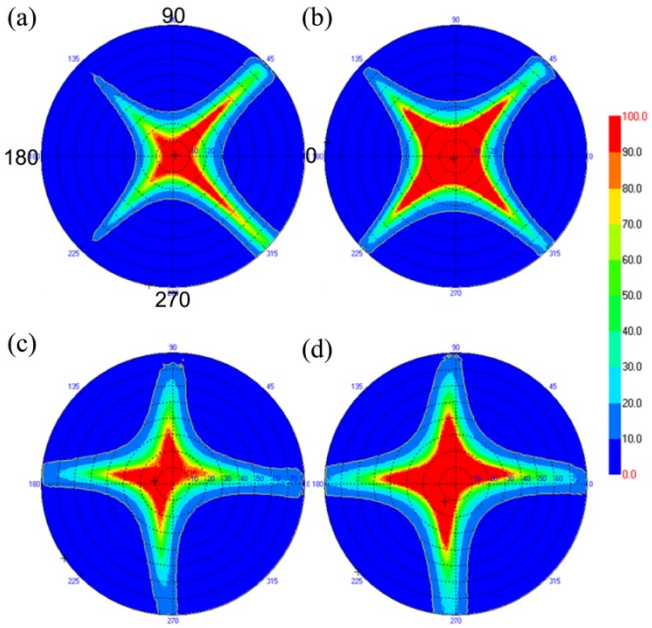

Figure 4. 6 Color-coded representation of iso-contrast characteristics of four types of the LC cells; (a) the HT LC cell without surface nanostructures, (b) the HT LC cell with surface nanostructures, (c) the TN LC cell without surface nanostructures, and (d) the TN LC cell with surface nanostructures. The iso-contrast map was measured at 4 V as a function of the azimuthal angle with respect to the input polarization of light for the normal incidence.

molecules on and around the surface nanostructures are much less profound in the HG geometry than in the HT geometry.

Another important issue is how the local LC alignment on the surface nanostructures affects the macroscopic EO properties such as the angular dependence of the EO transmission of the LC device from the symmetry viewpoint. Figures 4.6(a) and 4.6(b) show the iso-contrast characteristics of the HT LC cells with and without the surface nanostructures in color-coded representation, respectively. The angular dependence of the iso-contrast of the

LC cell was measured at 4 V as a function of the azimuthal angle with respect to the input polarization of light for the normal incidence. In fact, such iso-contrast map represents the viewing angle properties of the LC cell. Because two rubbing axes were anti-parallel to each other in the HT geometry used in this study, the viewing angles along only two directions (45^o and 315^o) were relatively large for the HT LC cell without the surface nanostructures. However, in the presence of the surface nanostructures, the viewing angles were more symmetric with respect to four directions (45^o, 135^o, 225^o, and 315^o) and substantially extended. As shown in Figs. 4.6(c) and (d), the viewing angle characteristics for the TN LC cell were substantially enhanced by the surface nanostructures. However, due to the intrinsic asymmetry of the EO properties and the narrow viewing angle characteristics of the TN LC cell, the symmetry enhancement was relatively limited compared to the HT LC cell. The examples of the two LC cells described above demonstrate that the local LC alignment on the surface nanostructures alters significantly the resultant EO properties of the LC device on a macroscopic scale without discrinations and/or defects observed in typical protrusion structures [71, 72].

4.4 Conclusion

It is developed a simple and powerful method of constructing the surface nanotopography with high mechanical stability based on thermal fixation of colloidal particles. The size-scalability and the mechanical stability of the

surface nanostructures were easily achieved by simply controlling the thermal treatment time. It was found that the theoretical predictions made in a simple model of the constant-volume agree well with the observed structural changes of the surface nanostructures by the thermal treatment. With the help of the surface nanostructures, it was demonstrated that the local LC alignment can be systematically controlled to increase the symmetry of the macroscopic EO properties of the LC devices, for example, the viewing angle characteristics of the HT and TN LC cells. Our colloidal-based surface nanotopography allows a viable scheme of manipulating the interfacial structural orders of a variety of functional materials including the LCs, polymers, and supported membranes on a nanometer-to-micrometer scale. Moreover, it would be applicable for various electrical and optoelectronic devices with surface nanostructures.

Chapter 5. Concluding Remarks

In this thesis, the constructions of the surface nanostructures and nanonetworks based on the self-assembled colloidal particles are presented. The applications of the surface nanostructures and nanonetworks are also demonstrated. Furthermore, it is presented that the basic principle of the self-assembly of colloidal particles and the interaction between the functional fluids formation with the template of self-assembled colloidal particle.

In Chap. 1, the general overview of the surface nanostructures and nanonetworks and the various construction methods are introduced. The general principles and key factors of surface nanostructures and nanonetworks formation are introduced. The construction method based on the self-assembled colloidal particles is also presented.

In Chap. 2, the construction of surface nanostructures and nanonetworks based on the liquid bridging phenomenon of functional fluids on self-assembled colloidal particles is demonstrated. Using the Ag ink which the Ag nanoparticles are dispersed in solvent as the functional fluid, the surface nanonetwork of metal mesh can be achieved. In addition, using the liquid bridging phenomenon, fluorinated polymer which thickness is in nano-range can be patterned on substrate. By applying the etching process, the contact area between the colloidal particle and substrate is etched while the other region is still remained. This method can construct various sizes of conducting nanonetworks by control the time of etching process and altering the size of

colloidal particles. Moreover, using the photoresistor and fluorinated polymer as the functional fluids to form the sacrificial layer of lift-off process, surface nanostructures of metal dots can be produces after the thermally deposition and removal of sacrificial layers. By control the coating conditions and using diverse kind of functional fluids, various size of nanomesh and nanodots can be constructed. Furthermore, based on the liquid bridging phenomenon, various functional fluids including polymer solution and nanomaterials dispersed in solvent with various sizes of colloidal based platform are applied to construct surface nanomesh and nanodots.

In Chap. 3, the deposited metal on the self-assembled colloidal particle is introduced. When the metal deposited on the self-assembled colloidal particles, the substrate can be applied as the optical lithographic mask. In addition, by detachment of colloidal particles after the metal deposition, the metal nanostructures are formed on substrate. For the practical applications, first, using the deposited metal on the self-assembled colloidal particle, the light can pass through the self-assembled colloidal particle with focusing effect due to the spherical shape of colloidal particle. Using such focusing effect, the size of photosensitization in photoresitor can be controlled. This method can construct various size of surface structure by regulating the metal thickness which can block the light. Second, using the surface metal nanostructure, the plasmonic biosensing application can be produced. Since the metal nanostructure of Au can generate the localized surface plasmon resonance in visible light range, the nanostructures made by detachment of colloidal particle can be applied to plasmonic biosensor. For the plasmonic

detection in biomimic environment, the supported lipid bilayers are formed on the substrate with surface metal nanostructure. The formation of supported lipid bilayers and the protein binding event can affect the plasmonic behavior that the plasmonic detection can be achieved.

In Chap. 4, it is presented the nanostructure for interaction with nanometerials. First, in order to obtain surface nanostructure using colloidal particle, the thermal treatment of colloidal particle is introduced. The thermal treatment induced with various times for strong fixation and size scalability of colloidal particle structures is presented. Using the constant volume model and spherical approximation, the structural dimension dependency of the induced time can be proved. Furthermore, for figuring out of the interaction between the surface nanostructures of thermally treated colloidal particles and liquid crystals, the substrates with nanostructure are assembled and the liquid crystals are filled in the cell. The iso-contrast characteristics can show the local distribution of liquid crystals on nanostructures.

In conclusion, through this thesis, it is presented that various construction methods based on the self-assembled colloidal particle. The colloidal particle with nano-range can applied as the surface nanostructure itself and it is also applied as the platform of the surface nanostructures and nanonetworks of the other materials. Approaches of basic principles which are the liquid bridging and thermally deformations, various sizes, shapes, distributions, and materials of surface nanostructures and nanonetworks can be constructed. In addition, not only the construction but also the application can be achieved, for example, interaction with liquid crystals, nanonetwork electrode, and

plasmonic biosensors. These construction methods of surface nanostructures and nanonetworks based on the self-assembled colloidal particle will provide a powerful platform for various applications in opto-electonic devices.

Bibliography

[1] E. Ozbay, *Science* **311**, 189 (2006).

[2] W. Khunsin, B. Brian, J. Dorfmuller, M. Esslinger, R. Vogelgesang, C. Etrich, C. Rockstuhl, A. Dmitriev, and K. Kern, *Nano Lett*. **11**, 2765 (2011).

[3] J. N. Anker, W. P. Hall, O. Lyandres, N. C. Shah, J. Zhao, and R. P. Van Duyne, *Nature Mater.* **7**, 442 (2008).

[4] V. M. Shalaev, W. Cai, U. K. Chettiar, H. -K. Yuan, A. K. Sarychev, V. P. Drachev, and A. V. Kildishev, *Optics Letters* **30**, 3356 (2005).

[5] J. Henzie, M. H. Lee, and T. W. Odom, *Nature Nanotech*. **2**, 549 (2007).

[6] W. Cai, U. K. Chettiar, A. V. Kildishev, and V. M. Shalaev, *Nature Photon.* **1**, 224 (2007).

[7] C. Lee and C. -J. Kim, *Phys. Rev. Lett.* **106**, 014502 (2011).

[8] J. H. Sung, J. Yu, D. Luo, M. L. Shuler, and J. C. March, *Lab Chip*. **11**, 389 (2011).

[9] G. M. Whitesides, *Nature* **442**, 368 (2006).

[10] L. -H. Hung, R. Lin, and A. P. Lee, *Lab Chip.* **8**, 983 (2008).

[11] A. D. McFarland and R. P. Van Duyne, *Nano Lett*. **3**, 1057 (2003).

[12] E. M. Larsson, J. Alegret, M. Kall, and D. S. Sutherland, *Nano Lett*. **7**, 1256 (2007).

[13] S. M. Marinakos, S. Chen, and A. Chilkoti, *Anal. Chem*. **79**, 5278 (2007).

[14] Y. Gao, B. Boulard, M. Lemiti, R. Rimet, P. Loeffler, and H. Poignant, *Journal of Non-Crystalline Solids* **256**, 183 (1999).

[15] M. Samuelsson, M. Armgarth, and C. Nylander, *Anal Chem*. **63**, 931 (1991).

[16] E. Hutter and J. H. Fendler, *Adv. Mater*. **16**, 1685 (2004).

[17] S. Donthu, Z. Pan, B. Myers, G. Shekhawat, N. Wu, and V. Dravid, *Nano Lett*. **5**, 1710 (2005).

[18] D. Attwood, G. Sommargren, R. Beguiristain, K. Nguyen, J. Bokor, N. Ceglio, K. Jackson, M. Koike, and J. Underwood, *Applied Optics* **32**, 7022 (1993).

[19] B. Li, X. Tang, H. Xie, and X. Zhang, *Sensors and Actuators A* **111**, 57 (2004).

[20] J. C. Hulteen and R. P. Van Duyne, *J. Vac. Sci. Technol. A* **13**, 1553 (1995).

[21] S. Zhang, *Nature Biotechnol.* **21**, 1171 (2003).

[22] P. Jiang and M. J. McFarland, *J. Am. Chem. Soc*. **126**, 13778 (2004).

[23] Y. Xia and G. M. Whitesides, *Annu. Rev. Mater. Sci*. **28**, 153 (1998).

[24] G. M. Whitesides, E. Ostuni, S. Takayama, X. Jiang, and D. E. Ingber, *Annu. Rev. Biomed. Eng*. **3**, 335 (2001).

[25] R. S. Kane, S. Takayama, E. Ostuni, D. E. Ingber, and G. M. Whitesides, *Biomaterials* **20**, 2363 (1999).

[26] X. Cheng, L. J. Guo, and P.-F. Fu, *Adv. Mater*. **17**, 1419 (2005).

[27] D. -G. Choi, S. G. Jang, H. K. Yu, and S. -M. Yang, *Chem. Mater*. **16**, 3410 (2004).

[28] R. A. Segalman, H. Yokoyama, and E. J. Kramer, *Adv. Mater*. **13**, 1152 (2001).

[29] S. -W. Lee, S. C. Park, Y. Lim, B. Lee, and S. –D. Lee, *Adv. Mater*. **22**, 4172 (2010).

[30] S. Reyntjens and R. Puers, *J. Micromech. Microeng.* **11**, 287 (2001).

[31] S. -M. Yang, S. G. Jang, D. -G. Choi, S. Kim, and H. K. Yu, *Small* **2**, 459 (2006).

[32] Y. Cui, M. T. Bjork, J. A. Liddle, C. Sonnichsen,B. Boussert, and A. P. Alivisatos, *Nano Lett*. **4**, 1093 (2004).

[33] H. Kim, J. Kim, H. Yang, J. Suh, T. Kim,B. Han, S. Kim, D. S. Kim, P. V. PIKHITSA, and M. Choi, *Nature Nanotech*. **1**, 117 (2006).

[34] J. L. Wilbur, A. Kumar, E. Kim, and G. M. Whitesides, *Adv. Mater*. **6**, 600 (1994).

[35] A. Bernard, J. P. Renault, B. Michel, H. R. Bosshard, and E. Delamarche, *Adv. Mater*. **12**, 1067 (2000).

[36] C. L. Haynes and R. P. Van Duyne, *J. Phys. Chem. B* **105**, 5599 (2001).

[37] A. S. Dimitrov, and K. Nagayama, *Langmuir* **12**, 1303 (1996).

[38] J. C. Hulteen and R. P. Van Duyne, *J. Vac. Sci. Technol. A* **13**, 1553 (1995).

[39] A. J. Ben-Sasson and N. Tessler, *Nano Lett*. **12**, 4729 (2012).

[40] J. Chen, W. -S. Liao, X. Chen, T. Yang, S. E. Wark, D. H. Son, J. D. Batteas, and P. S. Cremer, *ACS Nano* **3**, 173 (2009).

[41] B. K. Park, D. Kim, S. Jeong, J. Moon, abd J. S. Kim, *Thin Solid Films* **515**, 7706 (2007).

[42] X. Zhao, J. R. G. Evans, and M. J. Edirisinghe, *J. Am. Ceram. Soc.* **85**, 2113 (2002).

[43] H. Yoshida, Y. Ogawa, and Y. Kawai, *Appl. Phys. Lett*. **91**, 253901 (2007).

[44] T. Sekitani, Y. Noguchi, U. Zschieschang, H. Klauk, and T. Someya, *Proc. Natl. Acad. Sci*. **105**, 4976 (2008).

[45] H. Sirringhaus, T. Kawase, R. H. Friend, T. Shimoda, M. Inbasekaran, W. Wu, and E. P. Woo, *Science* **290**, 2123 (2000).

[46] S. -H Ko, H. Pan, C. P. Grigoropoulos, C. K. Luscombe, J.M.J. Fréchet, and D. Poulikakos, *Nanotechnology* **18**, 1 (2007).

[47] P. T. L. Koh, P. H. T. Uhlherr, and J. R. G. Andrews, *J. Colloid Interface Sci.* **108**, 95 (1985).

[48] F. Saija, F. Aliotta, M. E. Fontanella, M. Pochylski, G. Salvato, C. Vasi, and R. C. Ponterio, *J. Chem. Phys*. **133**, 081104 (2010).

[49] Y. -J. Na, S. -W. Lee, W. Choi, S. -J. Kim, and S. -D. Lee, *Adv. Mater.* **21**, 537 (2009).

[50] W. Choi, M. -H. Kim, and S. -D. Lee, *Jpn. J. Appl. Phys*. **50**, 080219 (2011).

[51] J. -H. Na, S. C. Park, Y. Sohn, and S. -D. Lee, *Biomaterials* **34**, 3159 (2013).

[52] A. Politano, V. Formoso, and G. Chiarello, *J. Nanosci. Nanotechnol.* **10**, 1313 (2010).

[53] E. M. Larsson, J. Alegret, M. Kall, and D. S. Sutherland, *Nano Lett*. **7**, 1256 (2007).

[54] F. Huo, G. Zheng, X. Liao, L. R. Giam, J. Chai, X. Chen, W. Shim, and C. A. Mirkin, *Nature Nanotech*. **5**, 637 (2010).

[55] G. Raschke, S. Kowarik, T. Franzl, C. So1nnichsen, T. A. Klar, and J. Feldmann, *Nano Lett*. **3**, 935 (2003).

[56] J. A. Adams, *Chem. Rev*. **101**, 2271 (2001).

[57] A. Schindlera, J. Brill, N. Fruehauf, J. P. Novak, and Z. Yaniv, *Physica E* **37**, 119 (2007).

[58] P. Lee, J. Lee, H. Lee, J. Yeo, S. Hong, K. H. Nam, D. Lee, S. S. Lee, and S. H. Ko, *Adv. Mater*. **24**, 3326 (2012).

[59] S. A. Maier, M. L. Brongersma, P. G. Kik, and H. A. Atwater, *Phys. Rev. B* **65**, 193408 (2002).

[60] W. J. Galush, S. A. Shelby, M. J. Mulvihill, A. Tao, P. Yang, and J. T. Groves, *Nano Lett*. **9**, 2077 (2009).

[61] S. Schelm and G. B. Smith, *J. Phys. Chem. B* **109**, 1689 (2005).

[62] R. H. Olsson and I. El-Kady, *Meas. Sci. Technol*. **20**, 012002 (2009).

[63] C. E. Talley, J. B. Jackson, C. Oubre, N. K. Grady, C. W. Hollars, S. M. Lane, T. R. Huser, P. Nordlander, and N. J. Halas, *Nano Lett*. **5**, 1569 (2005).

[64] B. -Y. Cao, M. Chen, and Z. -Y. Guo, *Phys. Rev. E* **74**, 066311 (2006).

[65] T. J. Merkel, S. W. Jones, K. P. Herlihy, F. R. Kersey, A. R. Shields, M. Napier, J. C. Luft, H. Wu, W. C. Zamboni, A. Z. Wang, J. E. Bear, and J. M. DeSimone, *Proc. Natl Acad. Sci*. **108**, 586 (2011).

[66] F. S. Yeung, J. Y. Ho, Y. W. Li, F. C. Xie, O. K. Tsui, P. Sheng, and H. S. Kwok, *Appl. Phys. Lett*. **88**, 051910 (2006).

[67] M. Woodson, and J. Liu, *J. Am. Chem. Soc*. **128**, 3760 (2006).

[68] T. -Y. Yoon, C. Jeong, S. -W. Lee, J. H. Kim, M. C. Choi, S. -J. Kim, M. W. Kim, AND S. -D. Lee, *Nature Mater*. **5**, 281 (2006).

[69] Y. Lu, Y. Yin, and Y. Xia, *Adv. Mater*. **13**, 34 (2001).

[70] J.-H. Na, H. Pae, J. Kim, C.-J. Yu, and S. –D. Lee, *Jpn. J. Appl. Phys*. **50**, 034101 (2011).

[71] W. -T. He, T. Nose, and S. Sato, *Mol. Cryst. Liq. Cryst*. **331**, 407 (1999).

[72] H. Yoshida, A. Takeda, Y. Taniguchi, Y. Tasaka, S. Kataoka, Y. Nakanishi, Y. Koike, and K. Okamoto, *Mol. Cryst. Liq. Cryst*. **410**, 255 (2004).

Publication

[1] International Journals

1. **S. C. Park**, I. -H. Lee, J. -H. Na, and S.-D. Lee, "Liquid-bridging in particle self-assemblies toward construction of periodic nano-mesh structures and nano-dot arrays", *Journal of Applied Physics*, submitted (2013).
2. **S. C. Park**, J. -H. Na, I. -H. Lee, X. Piao, N. Park, and S.-D. Lee, "Optical field focusing effect in hemispherical metal cap-on-dielectric particles for lithographic microstructures", *In preparation.*
3. **S. C. Park**, M. –H. Kim, I. -H. Lee, and S.-D. Lee, "Scalable conducting nanonetworks based on self-organized microparticles through selective etching", *In preparation*.
4. **S. C. Park**, D. Choi, I. –H. Lee, B. Lee, and S. -D. Lee, "Plasmonic Detection of Protein Binding in Supported Lipid Membranes on Periodic Metal Structures", *In preparation*
5. I. –H. Lee, **S. C. Park**, and S. –D. Lee, "Construction of 2-dimensional submicron holes and pillars using the Talbot effect through a phase-shift mask", *In preparation*.
6. J. –H. Na, **S. C. Park**, Y. –S. Choi, and S.-D. Lee, "Topographic confinement of a ferroelectric liquid crystal for highly efficient low-

voltage tunable electro-optic effect", *Applied Physics Express*, submitted (2013).

7. J. -H. Na, **S. C. Park**, Y. Sohn, S. -D. Lee, "Realizing the concept of a scalable artificial iris with self-regulating capability by reversible photoreaction of spiropyran dyes", *Biomaterials* **34**, 3159 (2013).
8. B. Lee, **S. C. Park**, M. –H. Kim, J. –Y. Kim, and S, -D. Lee, "Highly pressure-sensitive capacitive sensors based on porous elastomers for touch panel applications", *Journal of Information Display,* submitted (2013).
9. **S. C. Park**, J. -H. Na, and S.-D. Lee, "Colloidal particle-based surface nanotopography with high mechanical stability by thermal fixation for liquid crystal devices", *Journal of Applied Physics* **112**, 023104 (2012).
10. S. –W. Lee, J. –Y. Noh, **S. C. Park**, J. –H. Chung, B. Lee, and S.-D. Lee, "Biomimetic engineering of a generic cell-on-membrane architecture by microfluidic engraving for on-chip bioassay", *Langmuir* **28**, 7585 (2012).
11. J. –H. Na, **S. C. Park**, S. –U. Kim, Y. Choi, and S.-D. Lee, "Physical mechanism for flat-to-lenticular lens conversion in homogeneous liquid crystal cell with periodically undulated electrode", *Optics Express* **20**, 846 (2012).
12. J. –H. Hong, **S. C. Park**, S.-D. Lee, and Y.-W. Lim, "Unitary transflective liquid crystal display with an in-cell retarder on a wire

grid plate as a reflector-polarizer in a single driving configuration", *Japanese Journal of Applied Physics* **51**, 022201 (2012).

13. J. –H. Na, H. Li, **S. C. Park**, and S.-D. Lee, "Symmetric-viewing liquid crystal display with alternating alignment layers in an inverse-twisted-nematic configuration", *Journal of Information Display* **12**, 191 (2011).
14. S. –W. Lee, **S. C. Park**, Y. Lim, B. Lee, and S.-D. Lee, "Polymorphic meniscus convergence for construction of quasi-periodic assemblies and networks of colloidal nanoparticles", *Advanced Materials* **22**, 4172 (2010).
15. Y. –J. Na, T. –Y. Yoon, **S. C. Park**, B. Lee, and S.-D. Lee, "Electrically programmable nematofluidics with a high level of selectivity in a hierarchically branched architecture", *ChemPhysChem* **11**, 101 (2010).

[2] International Conferences

1. **S. C. Park**, I. -H. Lee, J. -H. Na, and S. -D. Lee, "Formation of Conducting Networks by Liquid-Bridging in Colloidal Self-Assemblies", 245th American Chemical Society (New Orleans, USA, 2013).
2. B. Lee, **S. C. Park**, M. –H. Kim, J. –Y. Kim, and S, -D. Lee, “Highly pressure-sensitive capacitive sensors based on porous elastomers for touch panel applications”, The 13th International Meeting on Information Display, (Exco, Korea, 2013).
3. [invited] S.-D. Lee, J. –H. Na, J. Kim, **S. C. Park**, S. –U. Kim, “Tunable liquid crystal-lens arrays for three-dimensional displays”, 4th Workshop on Liquid Crystals for Photonics . (Hong kong, China, 2012).
4. I. –H. Lee, **S. C. Park**, and S.-D. Lee, “Construction of periodic two-dimensional submicron pillars and holes using the talbot effect through a phase-shift mask”, International Symposium on Electronic/Optics Functional Molecules P-43 (Shanghai, China, 2012).
5. W. Choi, **S. C. Park**, C. –M. Keum, M. –H. Kim, and S. –D. Lee, “Sequential fabrication of multi-color pixel arrays in organic light emitting displays using transfer-printing sacrificial layer”, Materials Research Society Spring Meeting T5.15 (San Francisco, USA, 2011).

6. **S. C. Park**, J.-H. Na, and S.-D. Lee, “Immobilization of nanoparticles for fabrication of surface microstructures for wide-viewing liquid crystal displays”, Materials Research Society Spring Meeting O9.6 (San Francisco, USA, 2011).
7. [invited] S. –D. Lee, **S.C. Park**, Y. –S. Ryu, and S. –W. Lee, “Control of structural self-organization of colloids and lipids for optical applications”, Optics of Liquid Crystal 2011 PL-3 (Yerevan, Armenia, 2011).
8. **S. C. Park**, J. –H. Na, and S.-D. Lee, “Wide-viewing vertically-aligned liquid crystal displays with surface microstructure formation using colloidal particle”, The 11th International Meeting on Information Display p. 137 (Kintex, Korea, 2011).
9. J.-H. Na, **S. C. Park**, S.-U. Kim, and S.-D. Lee, “Tunable lenticular lens array using liquid crystal on periodically undulated electrodes for autostereoscopic 2D/3D convertible displays”, Tech. Digest 42th Soc. Inf. Display Int’l Sym. p. 1584 (Los Angeles, USA, 2011).
10. **S. C. Park**, S. –W. Lee, and S. –D. Lee, “Plasmonic biosensor for protein-binding on lipid membranes on a solid support with periodic metallic nanostructures”, 10th IEEE International Conference on Nanotechnology NKP-TS06-013 (Kintex, Korea, 2010).
11. Y. –T. Kim, J. –H. Hong, **S. C. Park**, Y. Kim, B. Lee, and S. –D, Lee, “Three-dimensional liquid crystal display with a monolithic elastomer substrate based on an integral imaging method”, The 23nd

International Liquid Crystal Conference 2.150 (Krakow, Poland, 2010).

12. S. –W. Lee, **S. C. Park**, S. –D. Lee, “Micropatterning of biological molecules through site-selective disassembly of supported lipid bilayers”, The 23nd International Liquid Crystal Conference 3.214 (Krakow, Poland, 2010).
13. S. –W. Lee, **S. C. Park**, S. –D. Lee, “Fabrication of self-aligned, hexagonal nanoparticle networks with the single particle width”, 238th American Chemical Society 294 (Washington DC, USA, 2009).
14. **S. C. Park**, S. –W. Lee, and S. –D. Lee, “Observation of protein-binding events on supported membranes by localized surface plasmon resonance”, 238th American Chemical Society 341 (Washington DC, USA, 2009).
15. S. –M. Cho, Y. –W. Lim, J. –H. Hong, **S. C. Park**, and S.-D. Lee, “Transflective liquid crystal display having an in-cell wire grid polarizer in a twisted nematic geometry”, International Symposium on Liquid Crystal Science and Technology p.65 (Kunming, China, 2009).
16. H. Pae, J. Kim, C. –J. Yu, **S. C. Park**, and S.-D. Lee, “Dynamic of two competing anchoring process of liquid crystals on photopolymer layers exposed to ultraviolet light”, 20th Korea-Japan Joint Forum on Organic Materials for Electronics and Photonics 28-008 (Chitose, Japan, 2008).

17. W. Choi, Y. –J. Na, **S C. Park**, and S.-D. Lee, “A high efficiency configuration of an organic light-emitting diode with surface microstructure” Materials Research Society Spring Meeting p.557 (San Francisco, USA, 2008).
18. C. Jeong, S. –W. Lee, **S. C. Park**. B. Lee, and S.-D. Lee, “Curvature-controlled organization of phase-separated domains in lipid monolayer” The 22nd International Liquid Crystal Conference p. 840 (Jeju, Korea, 2008).

[3] Domestic Conferences

1. **S. C. Park**, J. –H. Na, Y. –M. Song, and S. –D. Lee, “A simple method of surface microstructure formation using colloidal particles for wide-viewing liquid crystal displays”, 14th Korea Liquid Crystal Conference p.104 (Daegu, Korea, 2012).

초 록

최근, 표면나노구조물과 나노네트워크는 광학, 전자기학, 플라즈모닉스 및 포토닉스 등 다양한 분야의 핵심 요소로서 매우 많은 관심을 받고 있다. 표면 금속 나노 구조물은 다양한 비선형 광학, 예를 들어, 메타물질형성을 통한 광학 클로킹과 전자의 집단적 거동인 플라즈모닉 현상을 이용한 플라즈모닉 센서, 밴드 갭 조정을 이용한 광의 특이적 투과성 등을 유도할 수 있으므로 이러한 금속 나노 구조의 건설은 다양한 응용의 기본이 되는 핵심요인이 될 것이다. 또한 표면 금속 나노네트워크는 단순한 전극으로의 응용뿐만 아니라 유기발광다이오드 또는 유기태양전지 등의 전기-광학적 소자의 기능적인 요소로 응용될 수 있다. 따라서 이러한 다양한 분야의 적용가능하기 위해서는 다양한 크기와 모양 그리고 주기를 가지는 표면 나노구조물과 나노네트워크 형성기술에 대한 연구가 확립되어야 한다.

본 논문에서는 자기 조립된 콜로이드 입자를 기반으로 한 다양한 구조적 조건, 예를 들어 크기, 모양, 주기 등을 가지는 표면 나노구조물 및 나노네트워크 형성 방법을 제안하고 이러한 구조물을 이용한 다양한 응용을 논의하였다. 특히 콜로이드 입자와 기능성 물질 사이의 상호작용에 대한 물리적 메커니즘에 대하여 논의하였다. 이를 위하여 우선 표면나노구조물과 나노네트워크를

형성하는 다양한 기술에 대한 소개를 하고 상향식 방식인 자기조립 콜로이드 입자 기반의 형성기술에 대하여 논의하였다. 특히 형성하는 구조물의 구조적인 조건에 따른 형성기술의 방식에 관하여 논의하였다.

우선, 자기 조립된 콜로이드 입자를 하나의 형판으로 이용하여 다른 기능성 물질로 이루어진 표면나노구조물 및 나노네트워크 형성방식을 제안하였다. 액체-다리현상으로 알려진 방식을 이용하여 기능성 물질이 콜로이드 입자들 사이사이에 자발적으로 형성되었다. 이러한 액체-다리현상을 이용할 경우, 기능성 물질의 특성과 형판으로 이용되는 자기 조립된 콜로이드 구조의 크기 등이 상호 고려되어야 한다. 또한 이러한 기능성 물질의 자발적인 분포는 금속입자를 이용할 경우 나노그물모양의 구조물을 형성할 뿐아니라 다양한 폴리머를 이용할 경우 희생층으로 작용하여 리프트오프 공정에 적용되어 증착을 이용한 이차적인 금속물질의 나노닷 패턴에 이용된다. 한편, 이러한 기능성 물질을 금속전극 위에 형성할 경우 자발적으로 구조물이 형성된 기능성 물질이 식각 공정에 대한 희생층으로 작용하여 위치에 따른 차별적인 식각 공정이 가능하게 된다. 이러한 차별적인 식각 공정은 그 공정시간을 조절하여 다양한 크기를 가지는 구멍을 제작할 수 있다. 이러한 크기조절 가능한 금속 나노네트워크 전극의 경우 다양한 전기광학적 소자의 핵심부품으로 사용될 수 있다.

그리고 금속과 자기조립된 콜로이드 입자를 이용한 다양한 표면구조물 형성 방식에 대하여 연구하였다. 금속과 유전체는 다양한 광학적 특성을 가지므로 이러한 금속과 유전체가 함께있는 구조물을 형성하는 연구는 필수적이다. 자기조립된 콜로이드 입자에 금속층을 증착한후 콜로이드 입자를 제거하면 표면금속나노구조물을 형성할 수 있다. 자기 조립된 콜로이드 입자들은 밀집 단일 층을 형성하므로 이러한 밀집 단일 층의 경우 입자와 입자 사이의 공간은 기판이 노출된다. 따라서 이러한 노출된 기판은 금속을 증착하고 콜로이드 입자를 제거할 경우 금속나노구조물이 형성이 된다. 나노구형 식각 방식으로 알려진 이 방식은 입자의 크기를 변경할 경우 다양한 크기와 주기를 가지는 삼각형 모양의 표면 금속나노구조물을 형성할 수 있다. 이러한 표면금속나노구조물의 경우 플라즈모닉스나 포토닉스등의 핵심소자로 이용될 수 있다. 또한 자기조립된 콜로이드 입자에 금속을 증착하면 구면을 가지는 콜로이드의 입자의 특성상 입자를 통과한 빛은 수렴현상을 보이게 된다. 이러한 수렴현상은 광을 집속시키는 결과를 야기하므로 이러한 광의 집속은 광경화성 물질을 매우 작은 크기로 경화 시킬수 있다. 이러한 집속은 콜로이드 입자 윗부분에 증착된 금속 층을 통하여 조절할 수 있다. 이러한 광경화성 물질의 작은 크기로 경화시킨 기판을 이용하여

식각 공정 및 리프트오프 공정을 통하여 상호 반대되는 패턴을 가지는 기판을 제작할 수 있다.

또한 표면나노구조물 형성의 관점에서, 콜로이드 입자 그자체를 하나의 구조물로 적용하여 제작하였다. 열처리에 따른 콜로이드 입자의 구조적인 변화를 이용하여 열처리 정도를 조절하여 다양한 크기의 표면나노구조물을 제작하였다. 이러한 크기조절이 가능한 표면구조물을 나노물질과의 상호작용에 관한 연구를 위하여 적용하였다. 표면나노구조물은 나노물질, 즉 액정의 위치적인 거동을 변화시켜 다양한 광학적인 특성을 유도하였다.

결론적으로 본 논문에서는 다양한 크기와 모양 그리고 주기를 가지는 표면나노구조물 및 나노네트워크 형성 방식을 구현하였다. 이러한 다양한 구조적 조건을 가지는 표면나노구조물 및 나노네트워크 형성기술 및 그 배경원리는 다양한 전기광학적 소자 연구에 기반을 제공할 수 있을 것으로 기대된다.

주요어: 콜로이드 입자, 표면나노구조물, 표면나노네트워크, 계면상호작용, 전기광학소자, 바이오센서

학 번: 2007-20978